Copy
RM L57H08

NACA RM L57H08

NACA

RESEARCH MEMORANDUM

TRANSONIC INVESTIGATION OF AN AXIAL-FLOW COMPRESSOR ROTOR WITH A HUB-TIP RATIO OF 0.75 AND BLADES HAVING NACA A_2I_{8b} MEAN LINES

By Peter T. Bernot and Melvyn Savage

Langley Aeronautical Laboratory
Langley Field, Va.

NATIONAL ADVISORY COMMITTEE
FOR AERONAUTICS

WASHINGTON
September 30, 1957
Declassified January 12, 1961

NACA RM L57H08

NATIONAL ADVISORY COMMITTEE FOR AERONAUTICS

RESEARCH MEMORANDUM

TRANSONIC INVESTIGATION OF AN AXIAL-FLOW COMPRESSOR ROTOR WITH A HUB-TIP RATIO OF 0.75 AND BLADES HAVING NACA A_2I_{8b} MEAN LINES

By Peter T. Bernot and Melvyn Savage

SUMMARY

Blade-element analysis of a compressor rotor with blade sections having NACA A_2I_{8b} mean lines and 65-series thickness distributions has been performed at air-equivalent tip speeds up to 1,155 ft/sec. All tests were conducted in Freon-12 gas.

For all blade elements, minimum loss began to increase rapidly at an inlet Mach number of about 0.95. Angle of attack associated with minimum loss increased with speed becoming as much as 5° to 6° greater than the low-speed cascade design angle at the highest tip speed. Comparison with other compressor rotors indicates that use of thickness-chord ratios as low as practicable will delay the onset of increasing losses with Mach number. For air-equivalent tip speeds up to 116 percent of design, the measured values of turning angle agreed with the predicted cascade values at design angles of attack.

For the mean blade element, peak efficiencies of 90 percent and greater were obtained for speeds ranging from 90 percent to 122 percent of design speed. At the hub element, similar high values of peak efficiency were attained from 90 percent to 135 percent of design. A maximum peak efficiency of 89 percent was obtained at the tip element at design speed.

INTRODUCTION

A recent trend in axial-flow compressor design for turbojet engines has been the extension of flow-handling capabilities without an increase in frontal area. As a result, compressor blades are being subjected to Mach numbers ranging from high-subsonic to low-supersonic values. Blade

losses tend to increase rapidly with increasing Mach number within this range resulting in a detrimental effect on compressor efficiency. At the present time, investigations are being carried out in an attempt to determine which of the presently used blade sections is more nearly optimum for transonic applications. Numerous compressors designed for operation in the transonic regime have been built and tested with good results (for example, refs. 1, 2, and 3).

As a continuation of the present program, this paper presents additional blade-element data on the NACA A_2I_{8b} mean-line blade section (ref. 4) from tests of a compressor rotor incorporating this blade shape. The design and overall performance of this rotor have been reported in reference 5. The present paper includes the detailed blade-element performance.

Transonic conditions in this investigation were attained by testing the rotor at air-equivalent tip speeds up to 1,155 ft/sec which corresponds to a Mach number of about 1.20. Freon-12 gas was used throughout the entire program as the test medium.

SYMBOLS

C_p static-pressure-rise coefficient, $\frac{p_2 - p_1}{P_{1R} - p_1}$

c_p specific heat at constant pressure, ft-lb/slug $^{\circ}F$

D diffusion factor, $1 - \frac{V_{2R}}{V_{1R}} + \frac{\Delta V_\theta}{2\sigma V_{1R}}$

M Mach number

N rotor speed, rpm

P stagnation pressure, lb/sq ft

p static pressure, lb/sq ft

r radius, ft

T stagnation temperature, $^{\circ}R$

U blade speed, $\frac{\pi N r}{30}$, ft/sec

V velocity, ft/sec

W	gas weight flow, lb/sec
$W\frac{\sqrt{\theta}}{\delta}$	equivalent weight flow, corrected to sea-level conditions, lb/sec
α	angle of attack, angle between flow direction and blade chord, deg
β	gas flow angle, based on flow direction with respect to axial direction, deg
γ	ratio of specific heats
Δ	increase between stations 1 and 2
δ	ratio of inlet stagnation pressure at test conditions to NACA standard sea-level pressure, $\frac{P_1}{2,116}$
η_M	efficiency based on momentum considerations
θ	ratio of inlet stagnation temperature at test conditions to NACA standard sea-level total temperature, $\frac{T_1}{518.6}$
θ_o	rotor turning, $\beta_{1R} - \beta_{2R}$, deg
ρ	gas density, slug/cu ft
σ	solidity
$\bar{\omega}$	total-pressure-loss coefficient, $\frac{P_{1R} - P_{2R}}{P_{1R} - p_1}$

Subscripts:

d	design
h	hub
R	relative to rotor blade
t	tip
z	axial
θ	tangential

1 upstream of rotor

2 downstream of rotor

min minimum

A bar over parameter indicates mass-flow-weighted average.

ROTOR DESIGN

The rotor air design requirements including velocity diagrams have been reported in reference 5. However, for the sake of continuity, pertinent design variables will be repeated here, especially those values relating to blade-element considerations.

The test rotor had a diameter of 16 inches and was equipped with 20 blades having an average tip clearance of 0.030 inch. The annulus area at stations 1 and 2 is equal; the hub—tip-radius ratio at rotor inlet and outlet was 0.75. The rotor was designed to produce an overall pressure ratio of 1.258 with an efficiency of 92 percent at an air-equivalent tip speed of 808 ft/sec $\left(M_{1R} = 0.85\right)$.

Blade sections were comprised of the NACA A_2I_{8b} mean lines and 65-series thickness distributions. Maximum thickness varied from 8 percent at the tip to 10 percent at the hub. Other blade element design parameters are summarized in the following table:

	Tip	Mean	Hub
Radius ratio	1.000	0.875	0.750
Chord, in.	2.513	2.199	1.885
Inlet relative Mach number	0.850	0.771	0.697
C_p	0.397	0.466	0.532
D factor	0.429	0.519	0.618
p_2/p_1	1.241	1.224	1.197
V_{z2}/V_{z1}	0.91	0.91	0.91
Turning angle, deg	11.6	17.2	26.7
Inlet-air angle, deg	61.1	57.8	53.7
Angle of attack, deg	9.0	10.6	15.0
Blade isolated airfoil lift coefficient	7.3	11.3	18.5

The above angles are based on mean values of the rotor inlet and outlet axial velocities.

APPARATUS AND METHODS

Test Facility

A schematic drawing of the compressor test stand is presented in figure 1. A 250-horsepower dynamometer incorporating a 5.8:1 speed increaser was used to drive the test rotor. The recirculating gas flow was cooled by aircraft-type water radiators. Weight flow was varied by means of a drum-type throttle in conjunction with a butterfly valve which was located on the upstream face of the throttle. The drum-type throttle consisted of two concentric perforated cylinders, the inner being fixed while the outer was rotated by an electric actuator. By means of a gearing mechanism, rotation of the outer cylinder resulted in the movement of the butterfly valve.

Relocation of the test stand occurring after tests of reference 5 prompted several modifications which will be pointed out here. They are

(1) Installation of a new annular diffuser

(2) Addition of 23 straightening blades

(3) Relocation of throttle and radiators

(4) Use of curved ducting replacing the previous 90° angled ducts

(5) Installation of new inner and outer steel casings at the rotor test section

Since these modifications may have affected the overall characteristics of the test rotor, the overall performance results obtained from the present tests are included herein.

Instrumentation

Motor speed was determined by means of a commercial stroboscopic-type instrument into which was fed the output frequency of a small alternator coupled to the motor drive shaft. Apparatus for measurement of Freon purity is similar to that used in reference 5.

Four iron-constantan thermocouples mounted in the settling chamber were used to determine the inlet stagnation temperature. Temperature rise across the rotor was obtained by rakes having four doubly-shielded Chromel-Alumel thermocouples. Two rakes which covered the annulus area at the downstream survey station were wired with a third upstream rake in such a manner that the temperature difference could be measured and recorded electronically.

Inlet stagnation pressure was obtained from L-shaped total-pressure tubes mounted in the settling chamber. Upstream and downstream wall static pressures were measured by static orifices equally spaced about the circumference on inner and outer casings at each survey station. The survey stations were about 1 inch upstream and $1\frac{1}{2}$ inches downstream from the rotor. Detailed surveys of downstream static and total pressures as well as flow angle were obtained at 10 radial positions by means of a calibrated multiple-pressure probe shown in figure 2.

Data Reduction

Upstream radial variation of static pressure was assumed negligible since differences of outer and inner wall orifice measurements were small. Downstream static-pressure variation was determined from a curve which was faired through values obtained from the survey probe and wall orifices.

Mass flow was calculated at rotor inlet and outlet by integration of the elemental parameter ρV_z.

Overall total-pressure ratio was determined by mass-flow weighting the total-pressure values as measured by the survey probe. Overall efficiency based on momentum considerations was obtained by mass-flow weighting the blade-element efficiencies as indicated by the following formulas:

Blade-element efficiency,

$$\eta_M = \frac{c_p T_1 \left[\left(\frac{P_2}{P_1} \right)^{\frac{\gamma-1}{\gamma}} - 1 \right]}{U_2 V_{\theta 2}}$$

and overall efficiency,

$$\bar{\eta}_M = \frac{\int_{r_h^2}^{r_t^2} \eta_M \rho_2 V_{z2} \, d\left(r_2^2\right)}{\int_{r_h^2}^{r_t^2} \rho_2 V_{z2} \, d\left(r_2^2\right)}$$

As a check, an adiabatic efficiency based on measured total-temperature rise across the rotor was calculated for these tests but is not included herein. The temperature efficiency was found to be consistently lower than that presented. At the higher speeds, differences of about 5 percent were obtained while, at the lower speeds, the error

was appreciably greater, reaching as much as an 11-percent difference at the lowest test speed. The temperature-measuring apparatus apparently does not possess a high degree of accuracy when the temperature rise produced is low (on the order of 20°).

Test Procedure

The rotor was tested at eight speeds ranging from $0.90N_d$ to $1.43N_d$ employing Freon-12 gas as the testing medium. These speeds correspond to air-equivalent tip speeds ranging from 727 ft/sec to 1,155 ft/sec. Stagnation pressure in the settling chamber was maintained at a predetermined value by an automatic-control valve in the Freon supply system. The inlet stagnation pressure was held constant at 22 inches of mercury absolute except for the high-speed runs for which it was reduced as low as 16 inches to prevent overloading the drive motor. The inlet stagnation temperatures ranged from 60° F to 75° F.

At a given speed, the rotor surge point was determined by varying the flow by throttling from a fully opened setting to that at which surging occurred. Data were then taken for each of five or six throttle settings which covered the steady operating range of the rotor. All pressures were recorded by photographing a multitube mercury manometer board.

Validity of Data

A comparison between upstream and downstream measured weight flows is indicative of the quality of the flow measurements made. Figure 3 presents such a comparison. All test points are within ±3.0 percent except the near-surge points at 99 percent and 106 percent of design speed. It is to be noted that the majority of points fall within ±2.0 percent.

In this report, only the inlet weight flow values are presented. The downstream weight flow is considered to be less reliable because (1) it requires that pressure measurements are made in an oscillatory pressure field, (2) there is a variation in static pressure with radius which does not occur ahead of the rotor, and (3) accurate angle measurements are required whereas the inlet flow was known to be axial.

The reasonable agreement between the measured weight flows tends to indicate good reliability of the flow measurements taken and thereby permits a reliable blade-element performance analysis.

RESULTS AND DISCUSSION

Overall Performance

The overall performance of the rotor is presented in figure 4. The design values of pressure ratio and efficiency (1.258 and 0.92) were attained in these tests. A high level of efficiency (0.90 and greater) was maintained at speeds up to 122 percent of design. The pressure ratio is seen to increase generally with speed reaching a maximum value of 1.54 at the highest test speed. As usual, the range of weight flow decreases with increasing speed. These overall results show that somewhat higher pressure ratios and lower efficiencies were obtained than those reported in reference 5. Since the test rig as well as instrumentation techniques have been improved, the most recent data are considered to be the more accurate.

Blade-Element Performance

Blade-element performance is presented for three radial positions representing the tip, mean, and hub regions as follows:

Blade element	Radius, ft	Radius ratio	Annulus height from inner wall, percent
Tip	0.6444	0.966	86.6
Mean	.5810	.872	48.6
Hub	.5284	.793	17.0

The above radial locations for the tip and hub blade elements are considered to be sufficiently outside the wall boundary layer with the result that secondary flow effects are reduced to quite an extent. In addition, the streamlines and blade elements are assumed to lie along right circular cylindrical surfaces. In order to improve the accuracy of overall results, blade-element performance was computed for 10 centers of equal area.

The blade-element characteristics are presented in figure 5 as a function of angle of attack. Nine parameters are shown for each of the three radial stations previously mentioned. These parameters are inlet relative Mach number M_{1R}, flow turning angle θ_o, efficiency η_M, axial velocity ratio V_{z2}/V_{z1}, static-pressure ratio p_2/p_1, total-pressure ratio P_2/P_1, diffusion factor D, static-pressure-rise coefficient C_p, and total-pressure-loss coefficient $\bar{\omega}$. The design angle of attack based

on inlet-flow angle and blade-setting angle is indicated on these plots by an arrow on the abscissa scale.

Mean section.- Since the results at the mean section of the rotor give an average estimate of rotor performance, these results are discussed first (figs. 5(a) and 5(b)).

From the plots of efficiency, all test points at the three lowest speeds show operation at values greater than or equal to 0.90. Peak efficiency at each speed occurs at angles of attack greater than the low-speed cascade design value (arrow on abscissa) in all cases. For the N/N_d range of 0.90 to 1.16, this difference in angle of attack varies from 1° to about 3.5°, while for the higher speeds the difference increases to about 6°. The highest relative inlet Mach number for which the efficiency was at least 0.90 was 0.96 and occurred at a value of $N/N_d = 1.27$.

Referring to the total-pressure-loss coefficient $\bar{\omega}$, low values (below 0.07) of minimum loss were obtained for $N/N_d = 0.90$ to 1.22. At greater speeds (corresponding to higher inlet Mach number), minimum loss increases rather rapidly, attaining values of 0.21 and 0.26 at values of N/N_d of 1.35 and 1.43, respectively. This is due mainly to the greater loss levels associated with higher inlet relative Mach number and is in accord with high-speed cascade tests. (See fig. 80 of ref. 6.) Variation of angle of attack associated with minimum loss exhibits a similar trend to the peak efficiency previously discussed. With increasing speed, angle of attack at minimum loss generally increases and is seen to reach a value of 14° at the highest speed. This trend is in agreement with previous transonic compressor tests (refs. 1, 2, and 3).

The total-pressure ratio is seen to increase with angle of attack at each speed as expected. For values of $N/N_d = 1.16$ and 1.27, low values of pressure ratio are noted at the lowest angle of attack obtainable. This effect is probably due to choking effects as evidenced by high loss and resulting low efficiency. Values of peak total pressure generally increase with speed, but at speeds greater than $N/N_d = 1.16$, this trend is not so pronounced as that which occurred at lower speeds. The peak total-pressure ratio obtainable at an efficiency of at least 0.90 was 1.47 at $N/N_d = 1.27$.

The estimated rotor-turning-angle variation with angle of attack was extrapolated from low-speed cascade data of references 4 and 7 and is presented as dashed lines in the θ_o plots. Test values of turning angle for the four lowest speeds agree within $\pm 1^\circ$ at the design angle of attack. At angles of attack greater than design, the turning angle is seen to increase almost linearly which does not agree with trends predicted by cascade data. Design angle of attack was not obtained at speeds greater than $N/N_d = 1.16$ because of test stand limitations and therefore a useful comparison cannot be made.

Effects of blade loading are characterized by plots of static-pressure-rise coefficient C_p, and diffusion factor D. In general, both parameters exhibit the same trends. At $N/N_d = 1.16$, the level of C_p begins to decrease indicating that the blade loading is starting to become excessive. The same is true for the diffusion factor which is seen to decrease to some degree at $N/N_d = 1.22$. At design angle of attack and design speed, the test values of D and C_p were higher by about 0.05 than their respective design values.

The static-pressure ratio across the rotor is seen to increase with speed up to $N/N_d = 1.22$. However, as speed is increased further, the pressure-ratio level decreases which indicates that the magnitude of the loss levels has become large. At this higher speed range, the inlet Mach numbers are 0.95 or greater. With the apparent existence of a shock-wave pattern, the increasing loss levels are to be expected.

An examination of the axial velocity ratio variation shows a gradual decrease of the minimum values for N/N_d of 0.90 to 1.16. This effect is expected because the work output is increasing while the efficiency variation is relatively small. The levels of velocity ratio are seen to increase appreciably at the three highest speeds. This trend would seem to indicate separation at the tip or hub sections or both thus forcing the flow streamlines toward the mean section in either event.

Hub section.- As reported in reference 8, the boundary layer on the blade surface is centrifuged outward along the blade and as a result, measurements made at the hub-exit survey station probably do not give a true evaluation of the hub performance. In the following discussion on hub-element results (figs. 5(c) and 5(d)), this factor should be kept in mind.

Referring to the plots of efficiency, the angles of attack associated with peak efficiency are from 2.4° to 6.5° greater than the design angle of attack at speeds up to an N/N_d value of 1.27. At the two higher speeds, peak efficiency occurred at still higher angles of attack; however, the variation of efficiency is relatively small due to the restricted range of angle of attack obtainable. At speeds up to $N/N_d = 1.22$, values of efficiency were 0.90 or greater for all test points except the maximum flow condition at $N/N_d = 1.16$. The highest relative Mach number for which the efficiency was at least 0.90 was 0.93 and occurred at $N/N_d = 1.35$.

Variation of minimum total-pressure-loss coefficient is somewhat similar to that of peak efficiency. The angles of attack associated with minimum loss are greater than the design value and are seen to range from about 2.4° to 6°. Values of minimum loss coefficient are low (under 0.075) for speeds up to $N/N_d = 1.22$.

The levels of total-pressure ratio are generally higher than that shown at the mean section due mainly to the more efficient hub performance. Evidence of choked operation is again noted for the highest flow operating points at $N/N_d = 1.16$ and 1.27. The highest pressure ratio attained where the efficiency was at least 0.90 was 1.52 at $N/N_d = 1.35$.

The trends of axial velocity ratio are seen to be identical to those shown at the mean section. However, at the two highest speeds, the measured values are somewhat higher (about 1.10 as compared with 1.00). It is apparent that the loss regions at the outboard blade sections have displaced the streamlines resulting in the high V_{z2} values at the hub. On comparing mean- and hub-section performance, the increase in axial velocity ratio seems to have a beneficial effect.

Calculated values of rotor turning angle are seen to bunch closely together at speeds up to $N/N_d = 1.16$. The test values agree well with the predicted value for these speeds at the design angle of attack. Generally, the turning angles increase with angle of attack as noted at the mean section. Centrifuging of the blade boundary layer would tend to forestall blade separation resulting in higher turning. The minimum angle-of-attack test points for $N/N_d = 1.16$ and 1.27 indicate underturning of the flow since the hub section is operating in a choked condition.

For all test speeds, the trends of diffusion factor and pressure-loss coefficient are very similar to those exhibited at the mean blade element. At design conditions, the measured values of D and C_p are again higher than the design values by about 0.04 and 0.06, respectively.

The static-pressure-ratio level reaches maximum values at $N/N_d = 1.22$ as was the case with the mean section. A value of 1.19 which is just under the design value of 1.21 was obtained at design conditions.

Tip section.- Previous compressor experience has often shown the tip region to be the first to experience the adverse effects of high-speed operation. This fact is understandable since the inlet Mach number is higher and flow conditions are usually worse at the tip than those at the other blade positions. Analysis of blade-element losses associated with these tip effects may lead to the establishment of blade design criteria that delay the onset of large losses at high speeds.

From figures 5(e) and 5(f), values of peak efficiency are seen to occur near the design angle of attack for $N/N_d = 0.90$ to 1.06. At $N/N_d = 1.16$, the angle of attack associated with peak efficiency occurred about 3° above the design angle and is seen to increase with speed. The levels of efficiency at the three highest speeds are much lower than those obtained at the mean and hub sections. In fact, the maximum value attained was 0.89 at $N/N_d = 0.99$.

From the previous discussion, the total-pressure losses are expected to be rather high and this fact is confirmed by examining the loss curves. Angle of attack at minimum loss is seen to vary in a manner very similar to that of peak efficiency. Lowest values of pressure-loss coefficient were about 0.07 to 0.08 and occurred near the design angle of attack at the two lowest test speeds.

The trends exhibited by the total-pressure-ratio plots are generally similar to those shown at the mean section. At speeds greater than $N/N_d = 1.16$, the maximum pressure ratio remains essentially constant due to high losses at the higher inlet Mach numbers.

Test values of turning angle θ_o at low speeds agree favorably with those predicted at the design angle of attack. For the most part, however, underturning of the flow is seen to occur, the magnitude of which becomes greater with increasing angle of attack as well as with increasing speed. Piling up of the centrifuged blade boundary layer at the tip region would tend to reduce the effective camber of the blade resulting in low turning values.

For all test speeds save one, the axial velocity ratio decreases with angle of attack. This variation differs from that obtained at the mean and hub sections for speeds up to $N/N_d = 1.16$. The relatively higher losses at the tip section are indicative of a region of low-energy flow which would reduce in effect the outlet annulus area. Hence, the exit flow would tend to shift toward the rotor hub which explains the relatively higher values of axial velocity ratio obtained at the mean and hub blade elements. At speeds greater than $N/N_d = 1.16$, this effect is increased as indicated by the exceedingly low values of axial velocity ratio.

Variation of static-pressure-rise coefficient C_p is similar to that which occurred at the other blade sections; that is, values of C_p began decreasing at $N/N_d = 1.22$. At design speed, the lowest value of C_p was 0.465 which occurred at the design angle of attack and is somewhat greater than the design value of 0.397. The diffusion factor D increases with speed as expected. However, at $N/N_d = 1.22$ and greater, the diffusion factor is seen to stay at very high values (0.75 or more) with little or no tendency to decrease as noted for the previous blade sections. This behavior is probably due to the rather low values of V_{z2}/V_{z1} notably at the higher speeds which would result in high values of diffusion factor. Since the derivation of the diffusion factor (ref. 9) is based on subsonic Mach number considerations, the true worth of this parameter is questionable at Mach numbers greater than 1.0 unless the shock losses can be determined (see ref. 10). For this blade section, the inlet relative Mach number ranges from 0.99 to 1.17 for $N/N_d = 1.22$ to 1.43.

The static-pressure-ratio variation is very similar to that obtained at the mean and hub elements. The pressure-ratio level begins to decrease at $N/N_d = 1.27$ indicating the onset of flow breakdown. At design speed and angle of attack, a measured value of 1.22 was attained as compared with the design value of 1.235.

Radial variation.- In order to provide supplementary test data as an aid in analyzing rotor results, radial variations of several parameters are presented in figures 6 to 10 for all test speeds. These parameters are β_{1R}, M_{1R}, $\rho_2 V_{z2}$, η_M, and M_2. At a given speed, each curve presents measured data at a particular value of weight flow as indicated in the plots. The range of weight flows extends from the maximum obtainable to the minimum value near surge.

At $N/N_d = 0.99$, the design values of β_{1R} and M_{1R} were obtained (figs. 6 and 7) at the maximum weight flow of 36.9 pounds of Freon per second. The highest tip Mach number obtained in these tests was 1.21 while at the mean section ($r = 0.5833$ ft) the maximum value was 1.09.

Variation of outlet weight flow per unit area (fig. 8) at the tip region coincides with the high losses indicated previously by the blade-element plots. This condition becomes aggravated at higher speeds with the low-energy flow region expanding toward the mean radius. At $N/N_d = 1.35$ and 1.43, the peak values of mass flow occur near the hub section reaffirming the high values of V_{z2}/V_{z1} discussed and presented earlier in this paper.

The radial distribution of section efficiency (fig. 9) indicates trends somewhat similar to those exhibited by the mass-flow variations. The fall off at the tip region is in accord with the losses experienced at the tip which are relatively higher than those obtained at the more inboard sections. For all speeds up to $N/N_d = 1.22$ the section efficiencies are generally equal at the mean and hub blade regions. However, at greater speeds, the loss region has extended into the mean radius resulting in a large drop in efficiency. It is interesting to note the similarity of curves for maximum weight flow at $N/N_d = 1.16$ and 1.27. Since the weight flows are a maximum for these tests, this effect represents a more nearly choked rotor condition than those at the other speeds and therefore results in the lower efficiencies indicated.

Radial variation of absolute Mach number leaving the rotor is shown in figure 10. At design speed, the measured values agree fairly well with design at all weight flows. A maximum value of 0.77 was attained at the highest speed.

Minimum total-pressure loss.- In figure 11, the minimum values of total-pressure-loss coefficient for three stations are plotted against inlet relative Mach number. It can be seen that the level of loss

coefficients is generally higher for the tip section as expected. Values of loss coefficient for the three blade sections tend to become large (about 0.15) at a Mach number of approximately 0.95. In references 1 and 2, blade losses begin to rise rapidly at Mach numbers slightly greater than 1.0. This delay in loss rise was caused principally by the lower thickness-chord ratios of the aforementioned rotors. Mean radial values of thickness-chord ratio are 6.5 and 6.0 percent for these rotors as compared with 9.0 percent for the present rotor. The onset of loss rise can therefore be delayed by employing blade sections whose thickness-chord ratio is as low as practicable. Beyond Mach numbers of 0.95, losses increase at a rapid rate due in part to the growth of a shock-wave pattern discussed in reference 5.

D factor and C_p variation.- It can be recalled from the discussion of blade-element data, notably at the mean and hub blade sections, levels of C_p and D factor reach a maximum at a speed which is less than the highest test speed. The calculated C_p values required of the flow for an assumed constant efficiency would increase with speed. However, if the measured values deviate from the required condition, it becomes obvious that flow separation has occurred. Therefore, the establishment of maximum C_p values as design limiting parameters can be helpful for future design of rotors having configurations similar to the test rotor presented here.

Figure 12 presents minimum values of loss coefficient for each speed versus C_p and D factor at the three blade elements. Maximum values of C_p are seen to decrease from hub to tip blade sections. At the hub section, the highest value of C_p was 0.65 occurring at $N/N_d = 1.22$. The associated inlet Mach number was 0.85. For the mean section, the loss curve peaked at a C_p value of about 0.58 and occurred at the same speed as noted for the hub section. The inlet Mach number in this case was 0.92. It is suspected that the higher C_p value obtained at the hub section was due principally to a lower relative Mach number than that experienced at the mean section. Recalling that blade boundary layer tends to shift toward the outboard sections, it is also possible that losses chargeable to the hub section may have shifted. The limiting value of C_p at the tip section occurs at $N/N_d = 1.22$ reaching a value of 0.53. However, the loss coefficient is rather high as a value of 0.225 is indicated. Closer examination reveals that the losses begin to increase rapidly at a C_p value of about 0.47. The inlet relative Mach numbers associated with C_p values of 0.47 and 0.53 are 0.9 and 1.0, respectively. It is apparent that the indicated rising losses are caused by supersonic velocities existing on the blade suction surface resulting in a loss-producing shock system. In figure 6(b) of reference 2, variation of minimum loss coefficient at the tip region is presented in a similar manner and a lower value of limiting C_p (0.43) was obtained. Although

the tip blade camber and mean line of the rotor of reference 2 are very similar to that reported herein, it is felt that the lower C_p value was due mainly to differences of inlet relative Mach number. The Mach number associated with a C_p value of 0.43 in reference 2 was 1.10. In addition, it is to be noted that the thickness-chord ratio of the present rotor is twice that reported in reference 2. With such an appreciable difference, the effects of blade thickness should not be overlooked especially at Mach number near 1.0. Before a satisfactory design program based on C_p limiting values can be realized, it appears necessary to analyze many different rotors noting differences in blade shape, solidity, thickness, and Mach number.

In the plots of minimum loss coefficient versus D factor (fig. 12), the curves at the hub and mean section reach maximum values in a manner exhibited by the C_p plots. For the hub section, minimum loss coefficient begins to increase at a D factor of 0.76, while at the mean section, the value is 0.68. It is noted that these values occurred at $N/N_d = 1.22$ and were the maximum obtainable. For the tip section, the dashed lines represent a band of compiled rotor data reported in reference 9. The measured values of loss coefficient are seen to coincide with the bottom edge of this band. At a D factor of about 0.55, the loss coefficient begins to rise rapidly. The efficiencies related to the minimum loss coefficients at the tip section are all below 0.90.

SUMMARY OF RESULTS

A blade-element analysis has been performed on a compressor rotor having NACA A_2I_{8b} mean lines and 65-series thickness distributions at air-equivalent tip speeds up to 1,155 ft/sec with a maximum tip Mach number of 1.21. All tests were run using Freon-12 gas and the following results were obtained:

1. Blade losses for all sections began to increase quite rapidly at an inlet Mach number of about 0.95.

2. Angle of attack associated with minimum loss increased with speed, becoming as much as 5° to 6° greater than the low-speed cascade design angle at the highest tip speed.

3. For the mean element, peak efficiencies of 90 percent and greater were attained for speeds ranging from 90 percent to 122 percent of design speed. At the hub element, similar high values of peak efficiency were obtained from 90 to 135 percent of design. For the tip element, a maximum peak efficiency of 89 percent was obtained at design speed.

4. For speeds of 90 to 116 percent of design, the measured values of turning angle at design angle of attack agreed with those predicted from low-speed cascade data.

5. At angles of attack greater than design considerable overturning occurred at the mean and hub elements while at the tip element, underturning occurred because of the high losses especially at high speeds.

6. Comparison with other transonic rotors indicated that loss rise can be delayed by using thickness-chord ratios as low as practicable.

Langley Aeronautical Laboratory,
National Advisory Committee for Aeronautics,
Langley Field, Va., July 22, 1957.

REFERENCES

1. Montgomery, John C., and Glaser, Frederick W.: Experimental Investigation of a 0.4 Hub-Tip Diameter Ratio Axial-Flow Compressor at Transonic Inlet Relative Mach Numbers. II - Stage and Blade-Element Performance. NACA RM E54I29, 1955.

2. Felix, A. Richard, and Savage, Melvyn: Investigation of a High-Performance Axial-Flow Compressor Transonic Inlet Rotor Designed for 37.5 Pounds Per Second Per Square Foot of Frontal Area - Detailed Blade-Element Performance. NACA RM L56K23, 1956.

3. Boxer, Emanuel, and Bernot, Peter T.: Experimental Investigation of a Transonic Axial-Flow Compressor Rotor Designed for Sonic Inlet Velocity With an Inlet Hub-Tip Radius Ratio of 0.35. NACA RM L56F14, 1956.

4. Erwin, John R., Savage, Melvyn, and Emery, James C.: Two-Dimensional Low-Speed Cascade Investigation of NACA Compressor Blade Sections Having a Systematic Variation in Mean-Line Loading. NACA TN 3817, 1956. (Supersedes NACA RM L53I30b.)

5. Savage, Melvyn, Erwin, John R., and Whitley, Robert P.: Investigation of an Axial-Flow Compressor Rotor Having NACA High-Speed Blade Sections (A_2I_{8b} Series) at Mean Radius Relative Inlet Mach Numbers up to 1.13. NACA RM L53G02, 1953.

6. Dunavant, James C., Emery, James C., Walch, Howard C., and Westphal, Willard R.: High-Speed Cascade Tests of the NACA 65-$(12A_{10})10$ and NACA 65-$(12A_2I_{8b})10$ Compressor Blade Sections. NACA RM L55I08, 1955.

7. Felix, A. Richard: Summary of 65-Series Compressor-Blade Low-Speed Cascade Data by Use of the Carpet-Plotting Technique. NACA TN 3913, 1957. (Supersedes NACA RM L54H18a.)

8. Godwin, William R.: Distribution of Losses Behind a Compressor Rotor As Measured by a Rotating Rake. NACA RM L55F29, 1955.

9. Lieblein, Seymour, Schwenk, Francis C., and Broderick, Robert L.: Diffusion Factor for Estimating Losses and Limiting Blade Loadings in Axial-Flow-Compressor Blade Elements. NACA RM E53D01, 1953.

10. Schwenk, Francis C., Lewis, George W., and Hartman, Melvin J.: A Preliminary Analysis of the Magnitude of Shock Losses in Transonic Compressors. NACA RM E57A30, 1957.

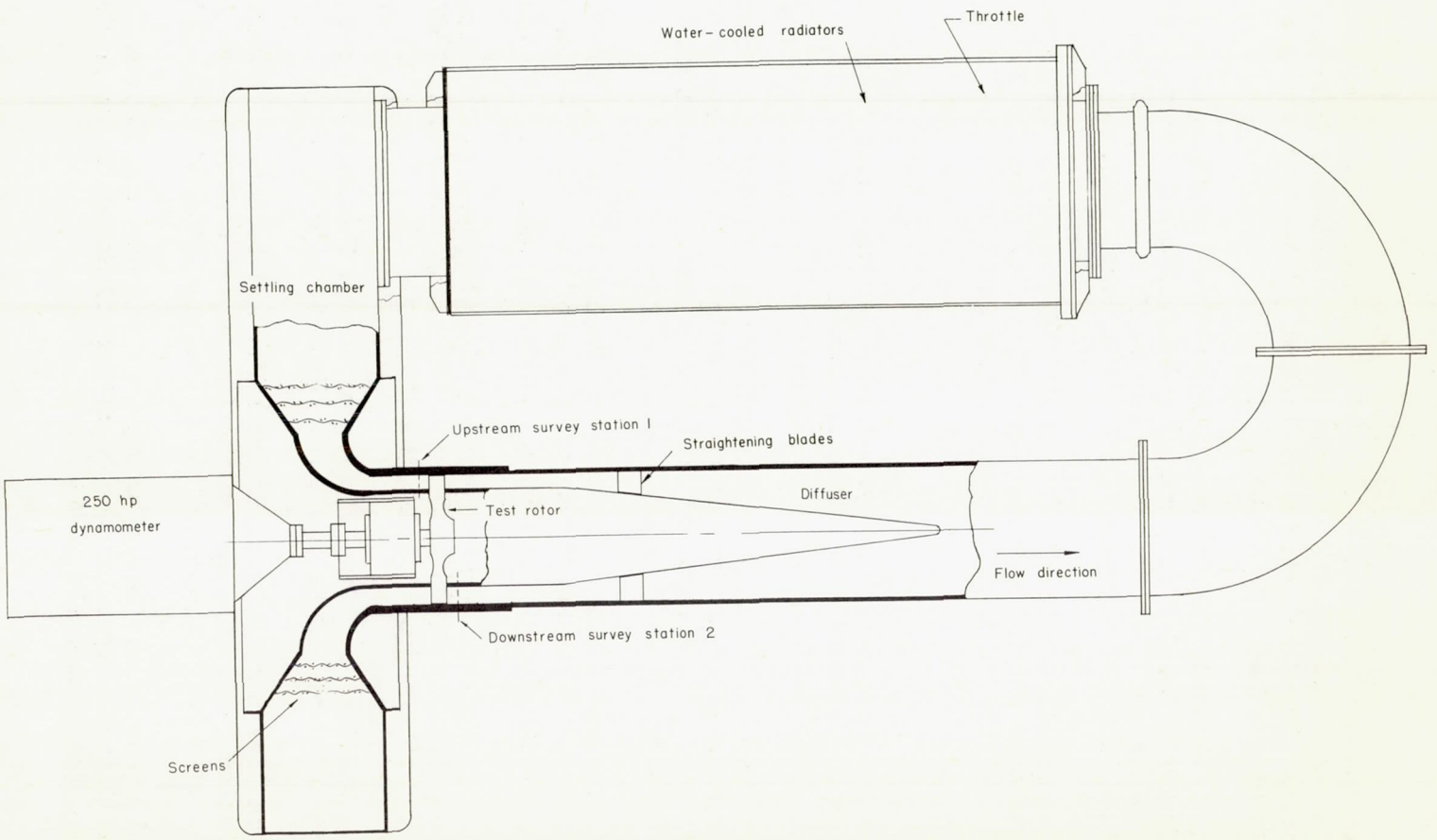

Figure 1.- Schematic drawing of compressor test stand.

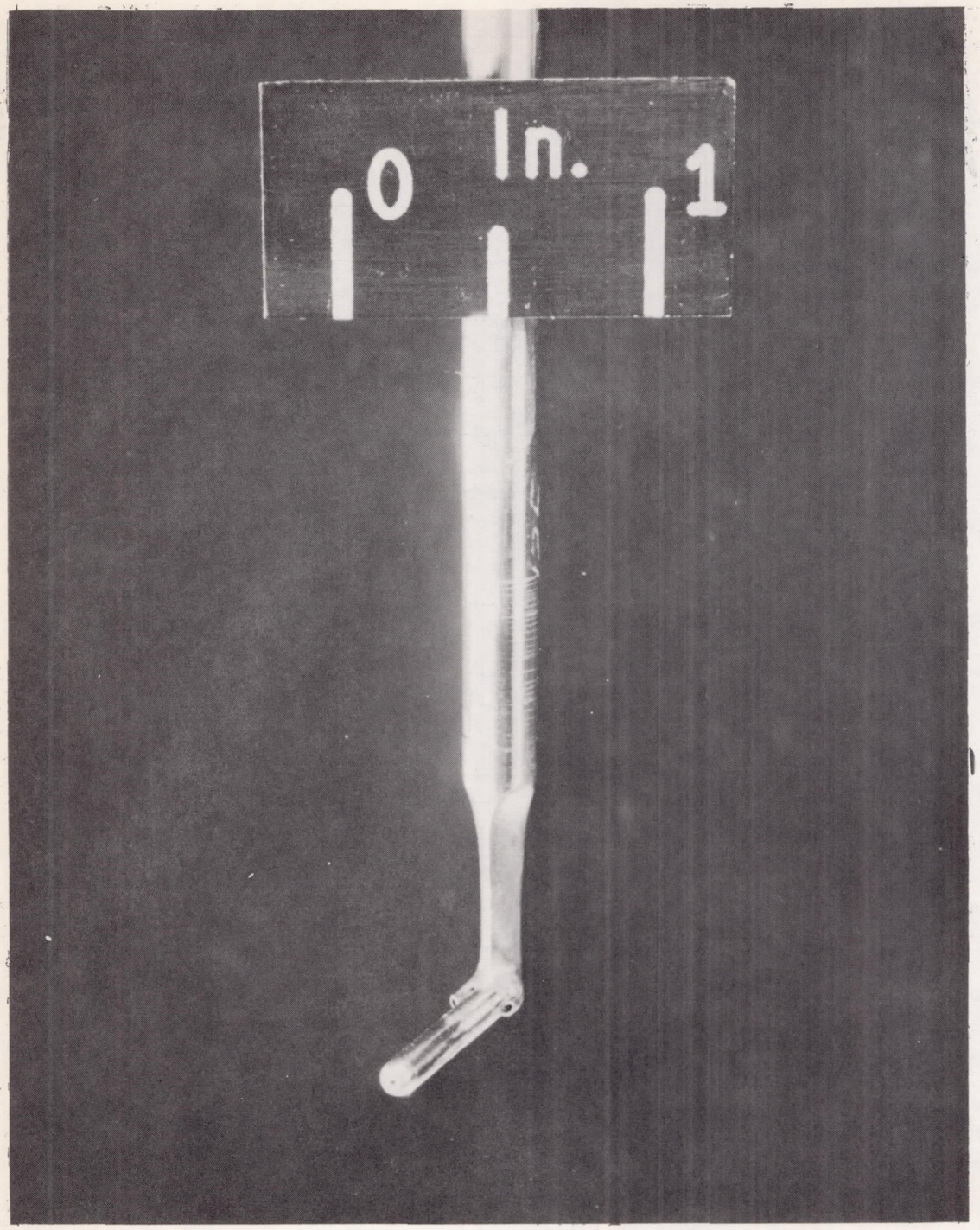

Figure 2.- Multiple-pressure survey probe. L-88798

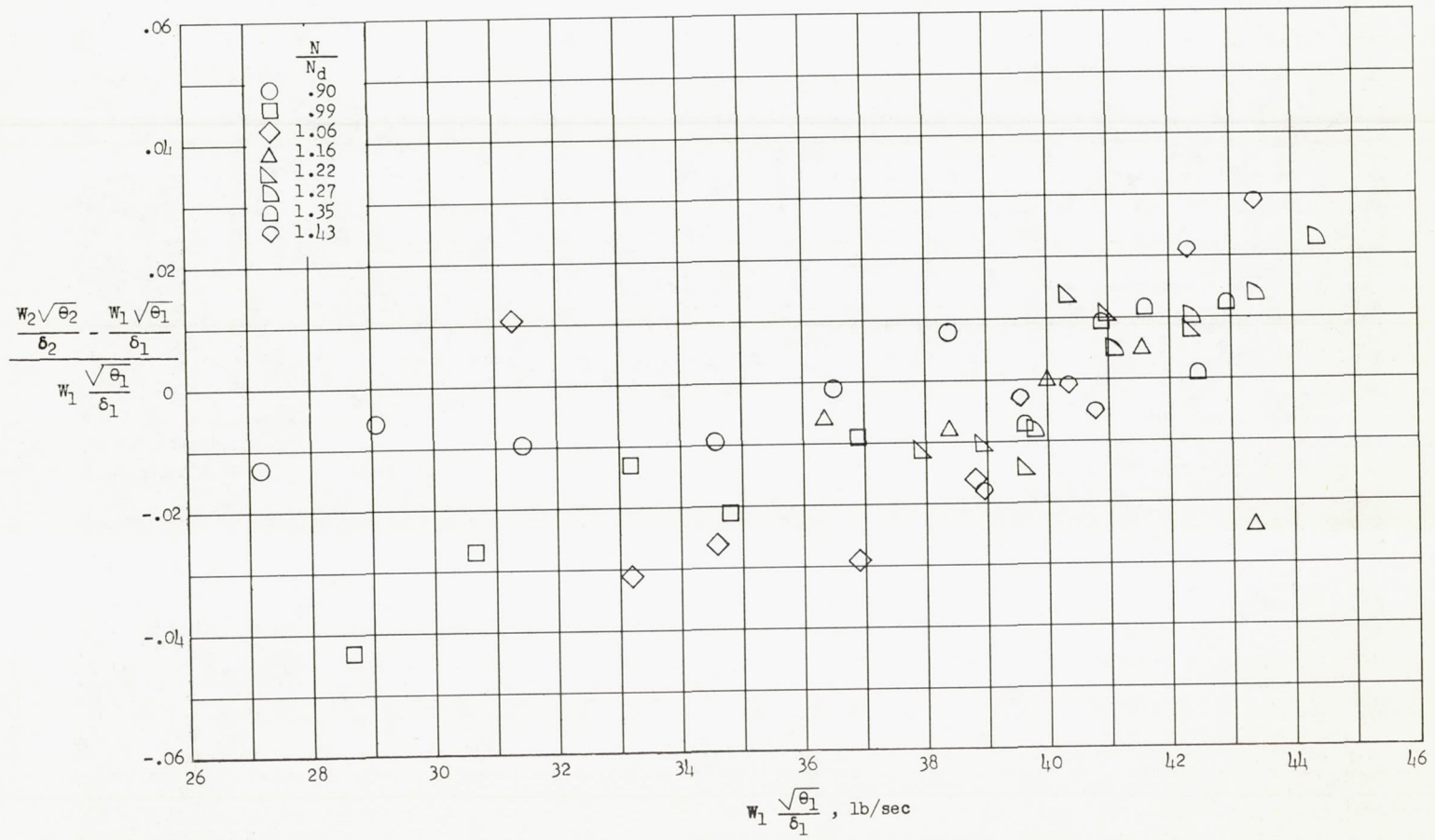

Figure 3.- Comparison of Freon weight flow measurements at various speeds.

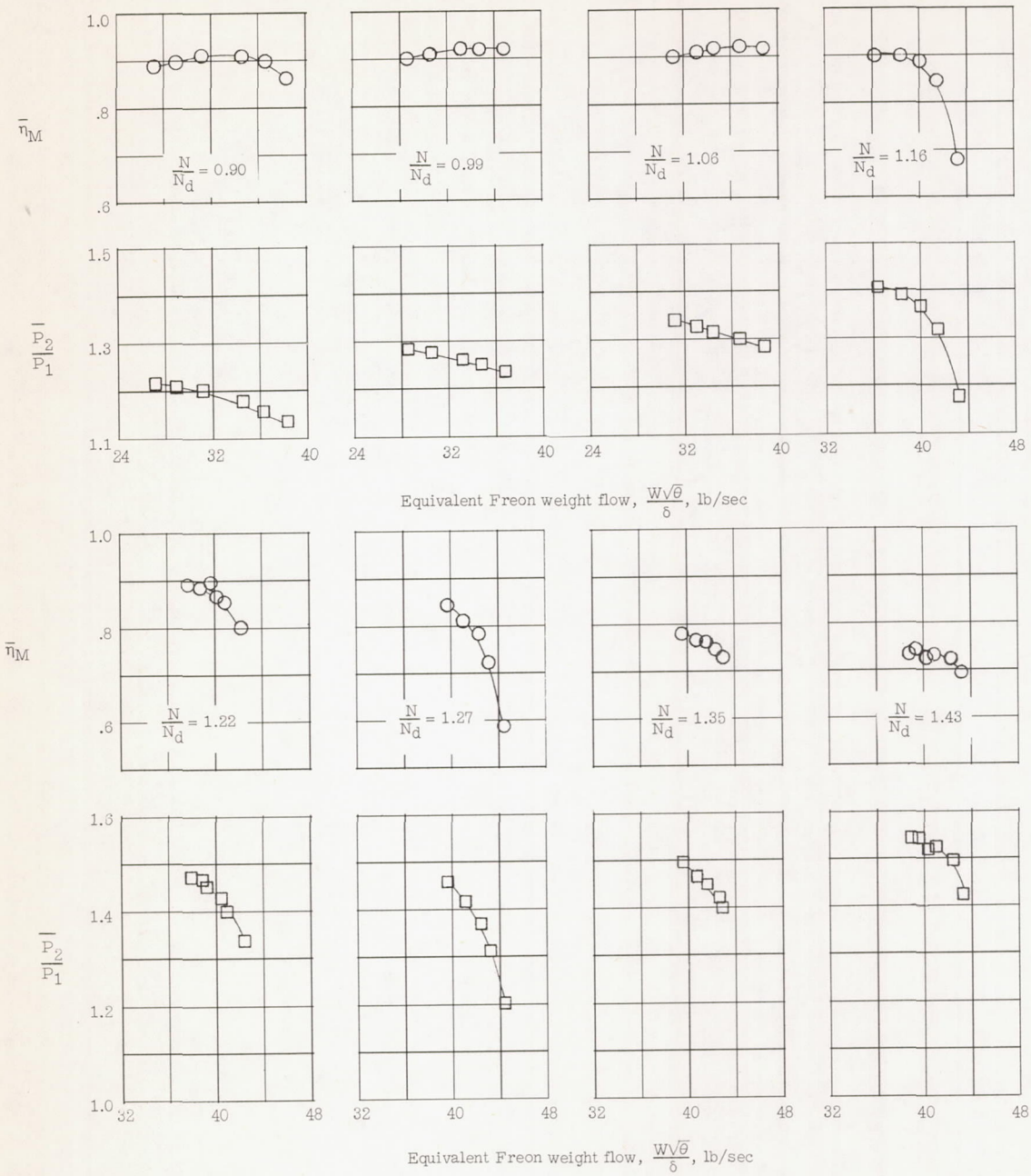

Figure 4.- Overall rotor performance.

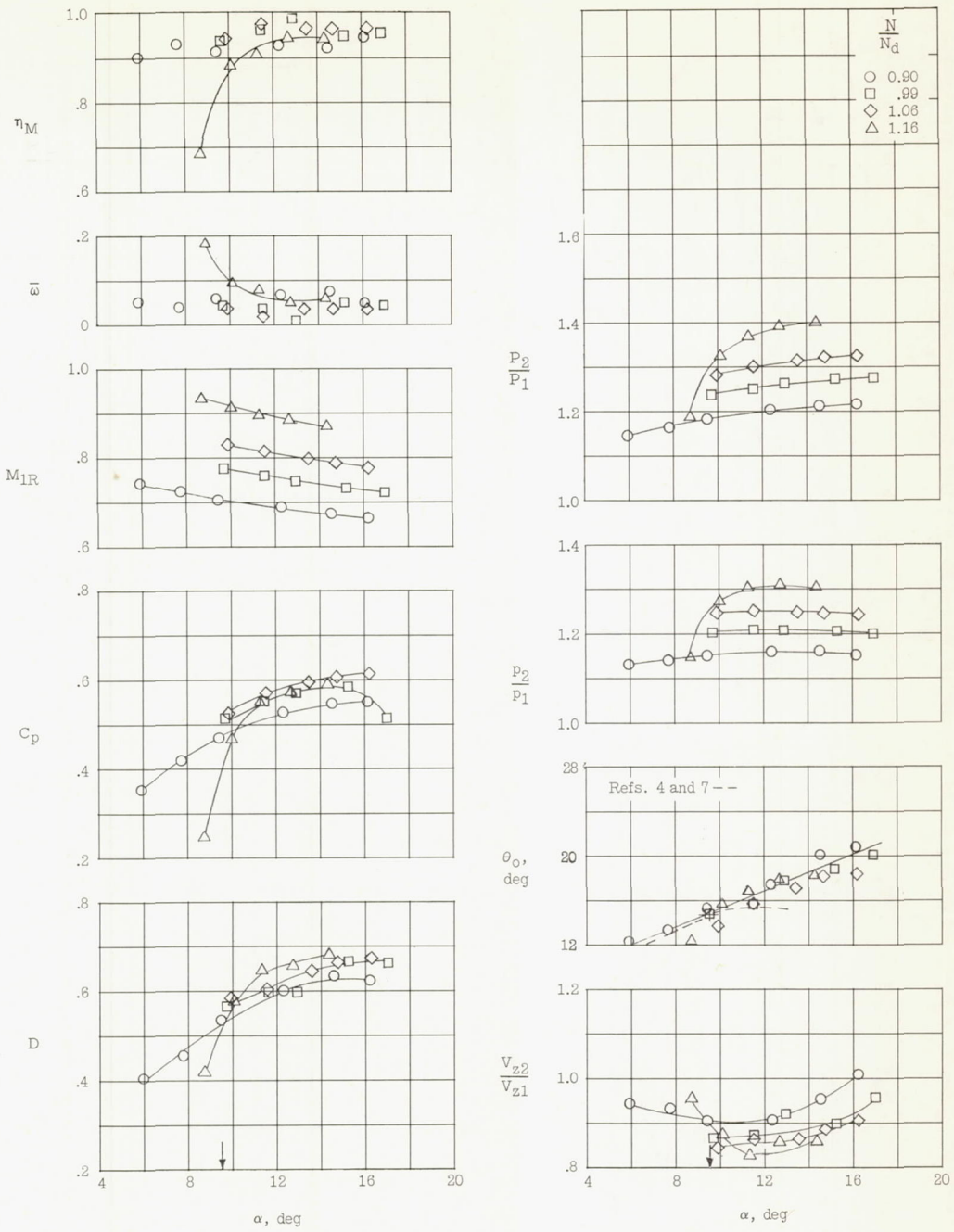

(a) Mean section, r = 0.5810 foot; $\frac{N}{N_d}$ = 0.90 to 1.16.

Figure 5.- Blade-element characteristics.

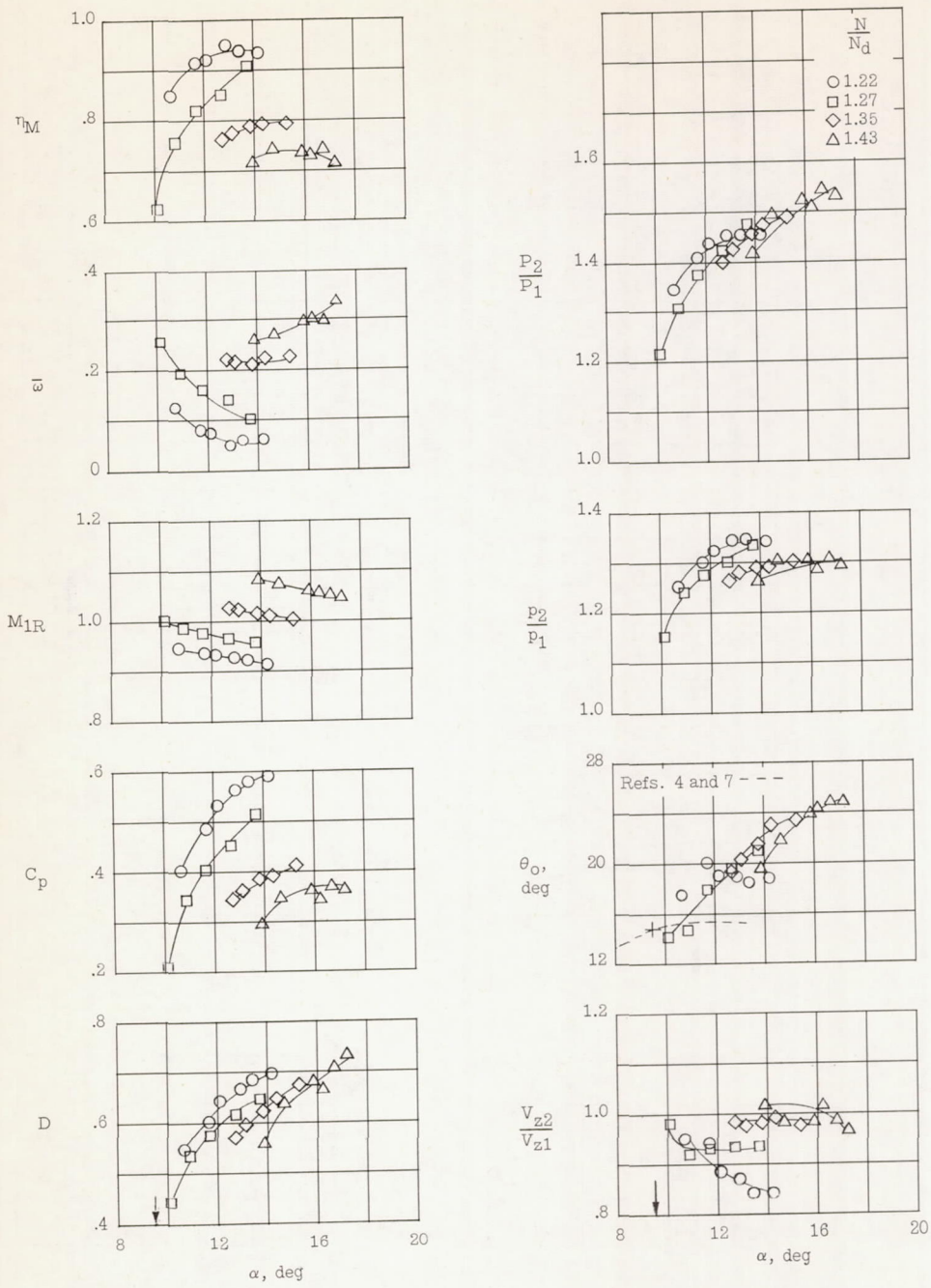

(b) Mean section, r = 0.5810 foot; $\frac{N}{N_d}$ = 1.22 to 1.43.

Figure 5.- Continued.

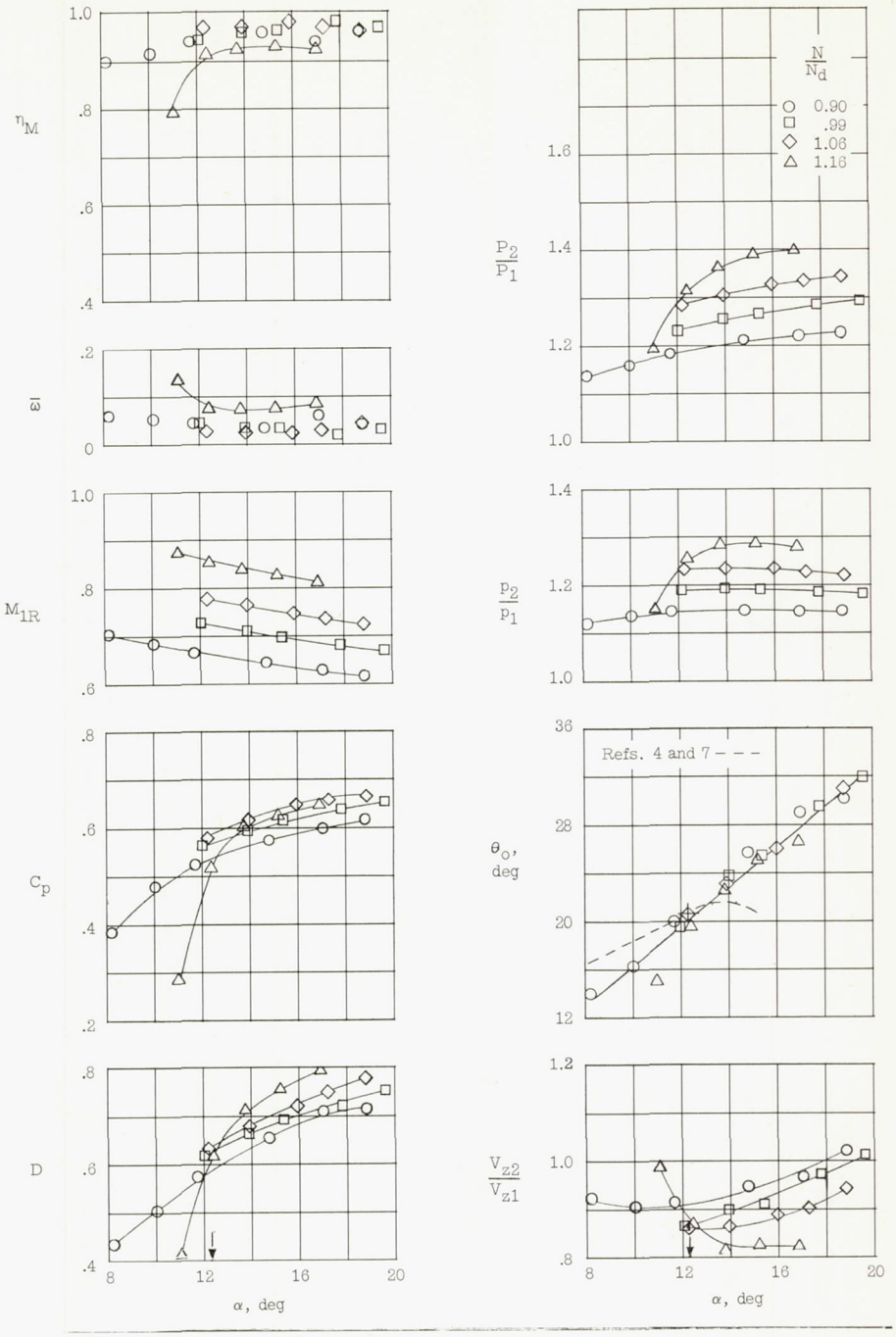

(c) Hub section, r = 0.5284 foot; $\frac{N}{N_d}$ = 0.90 to 1.16.

Figure 5.- Continued.

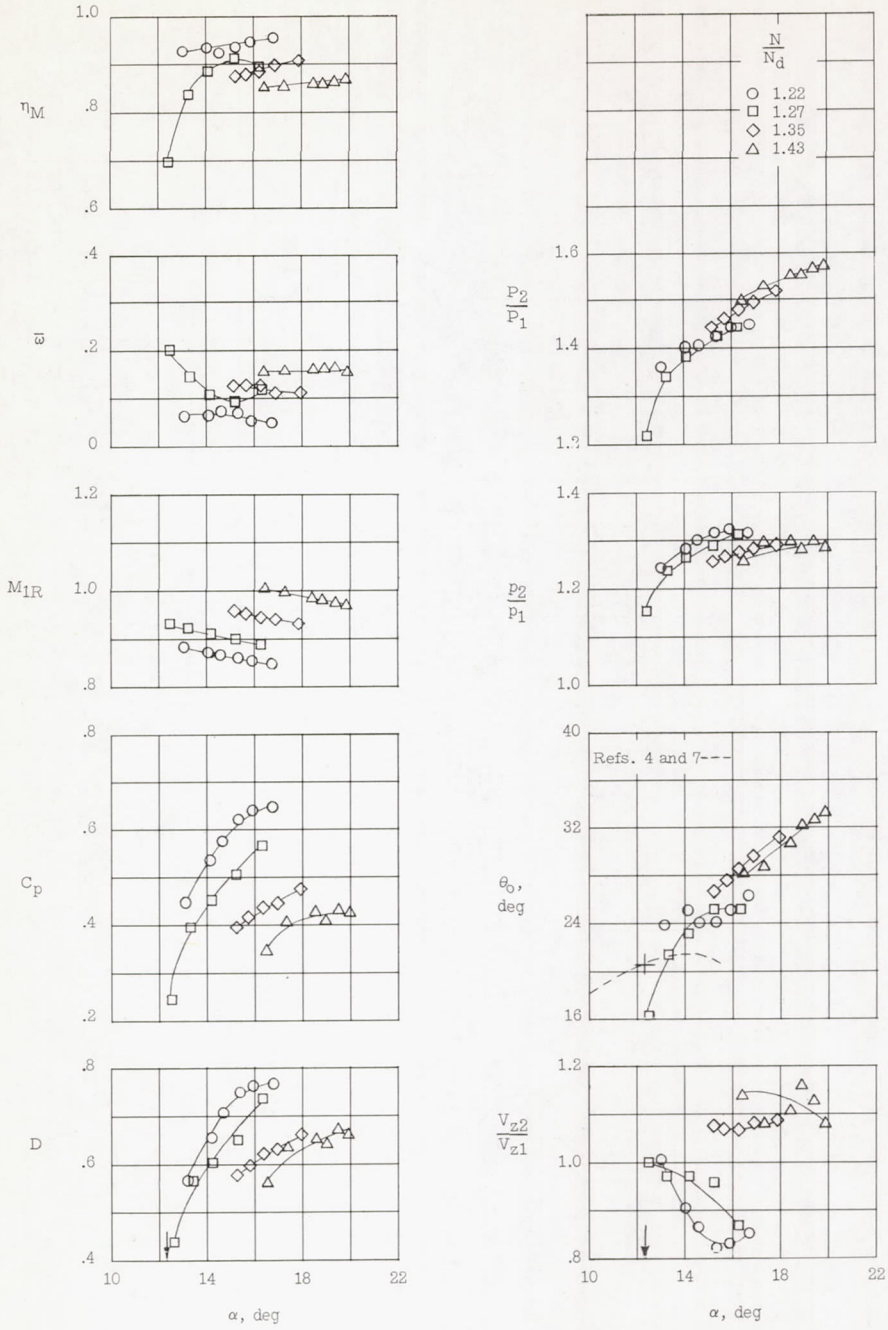

(d) Hub section, r = 0.5284 foot; $\frac{N}{N_d}$ = 1.22 to 1.43.

Figure 5.- Continued.

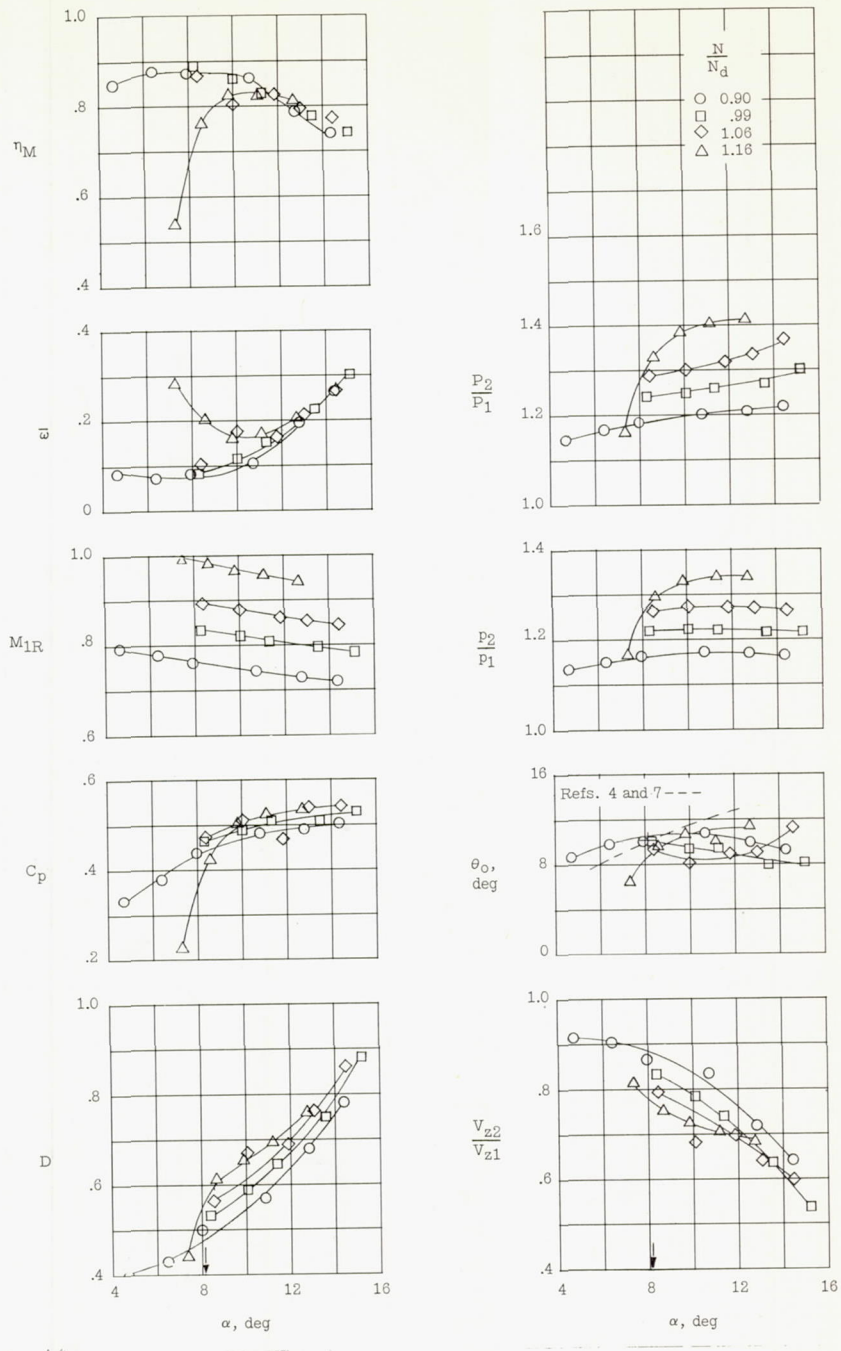

(e) Tip section, r = 0.6444 foot; $\frac{N}{N_d}$ = 0.90 to 1.16.

Figure 5.- Continued.

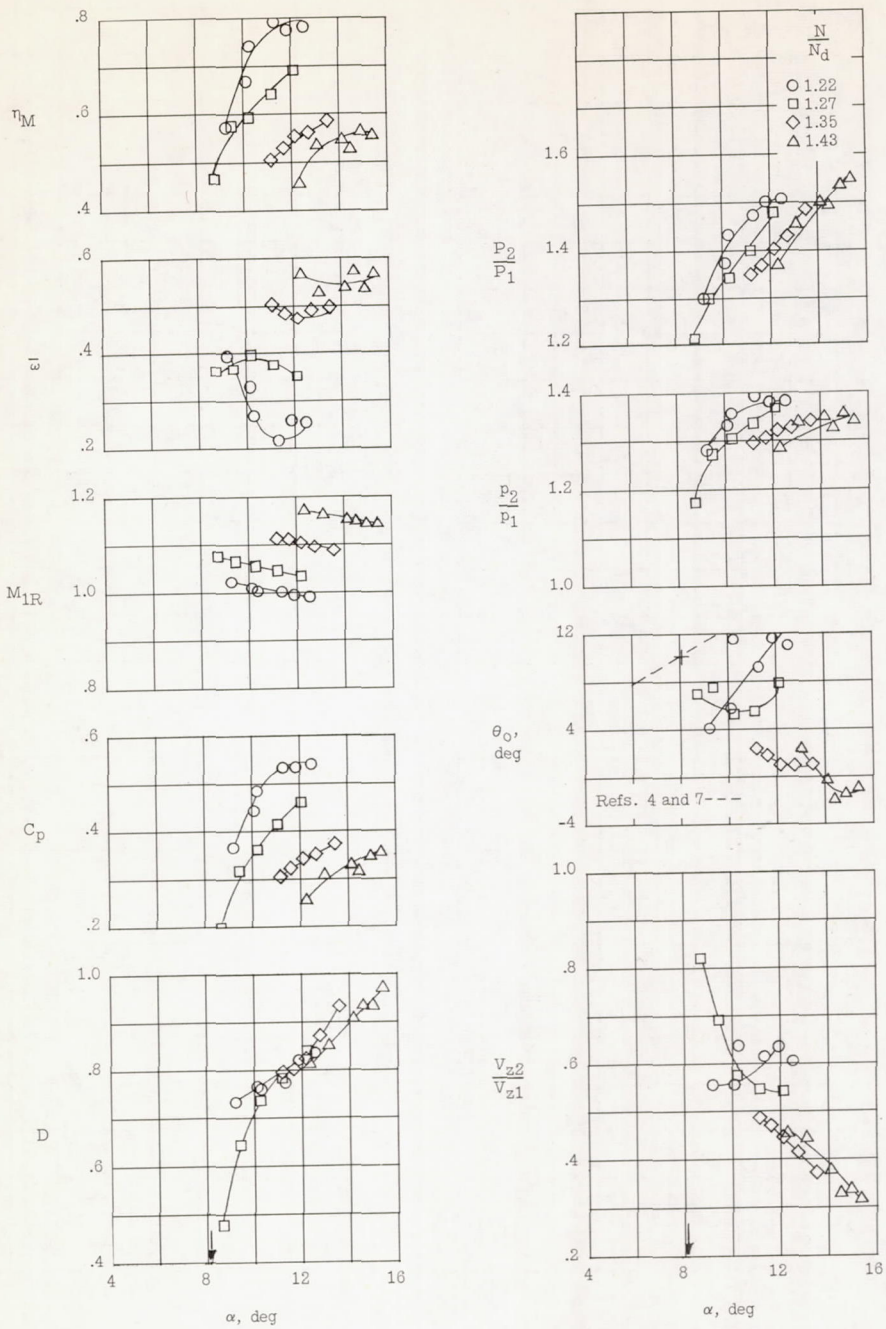

(f) Tip section, r = 0.6444 foot; $\frac{N}{N_d}$ = 1.22 to 1.43.

Figure 5.- Concluded.

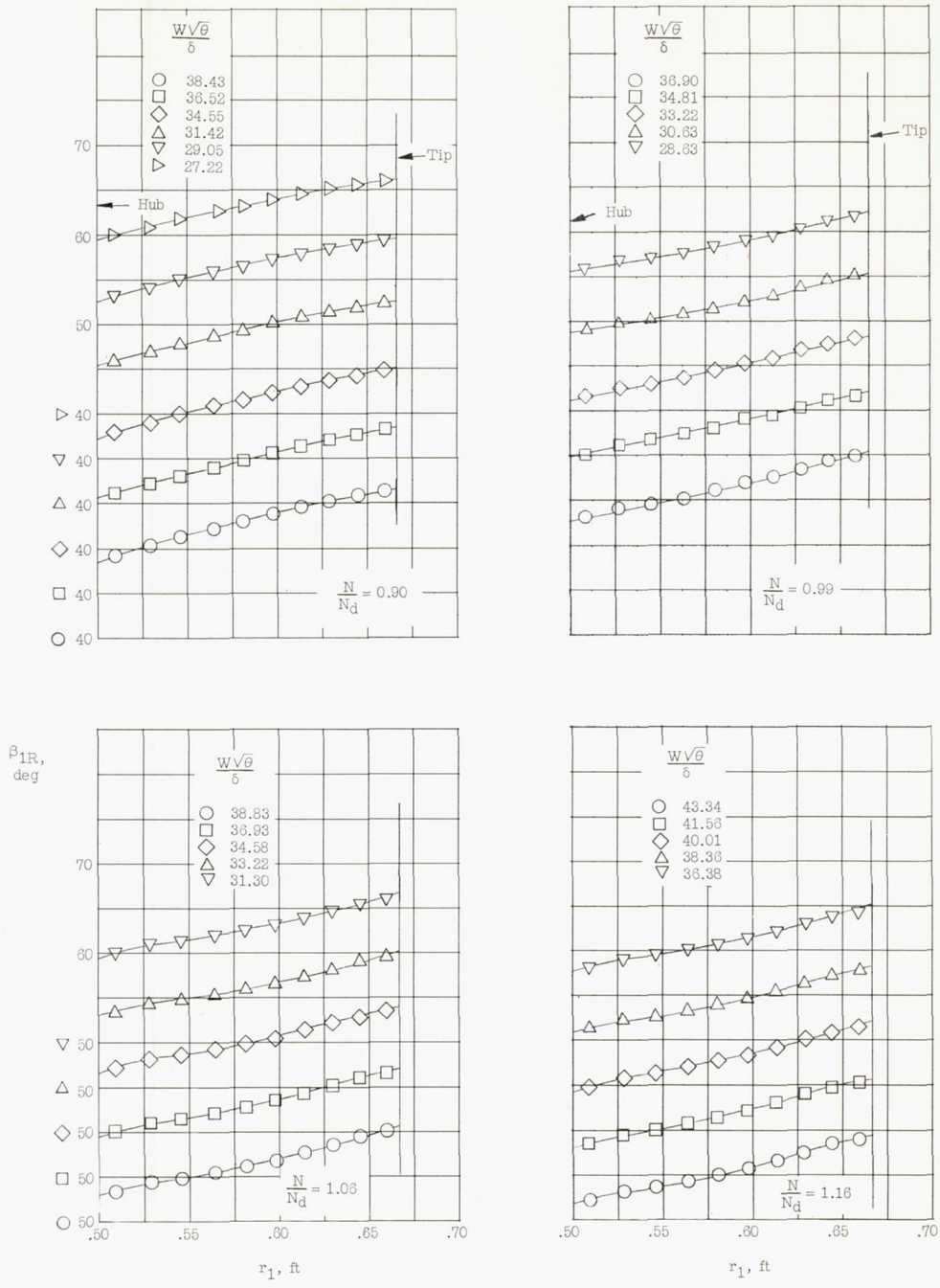

(a) $\frac{N}{N_d}$ = 0.90 to 1.16.

Figure 6.- Radial variation of relative inlet angle.

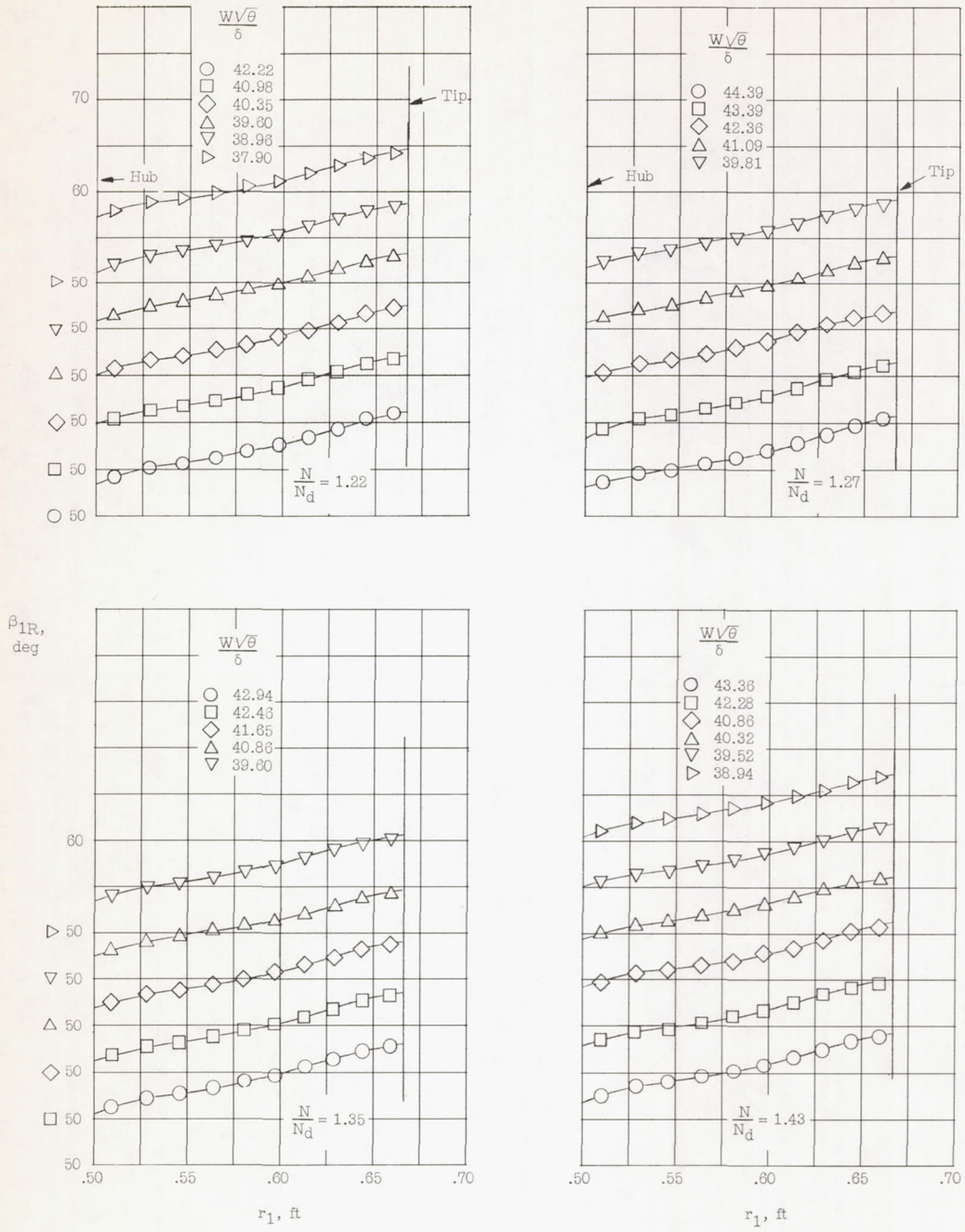

(b) $\frac{N}{N_d}$ = 1.22 to 1.43.

Figure 6.- Concluded.

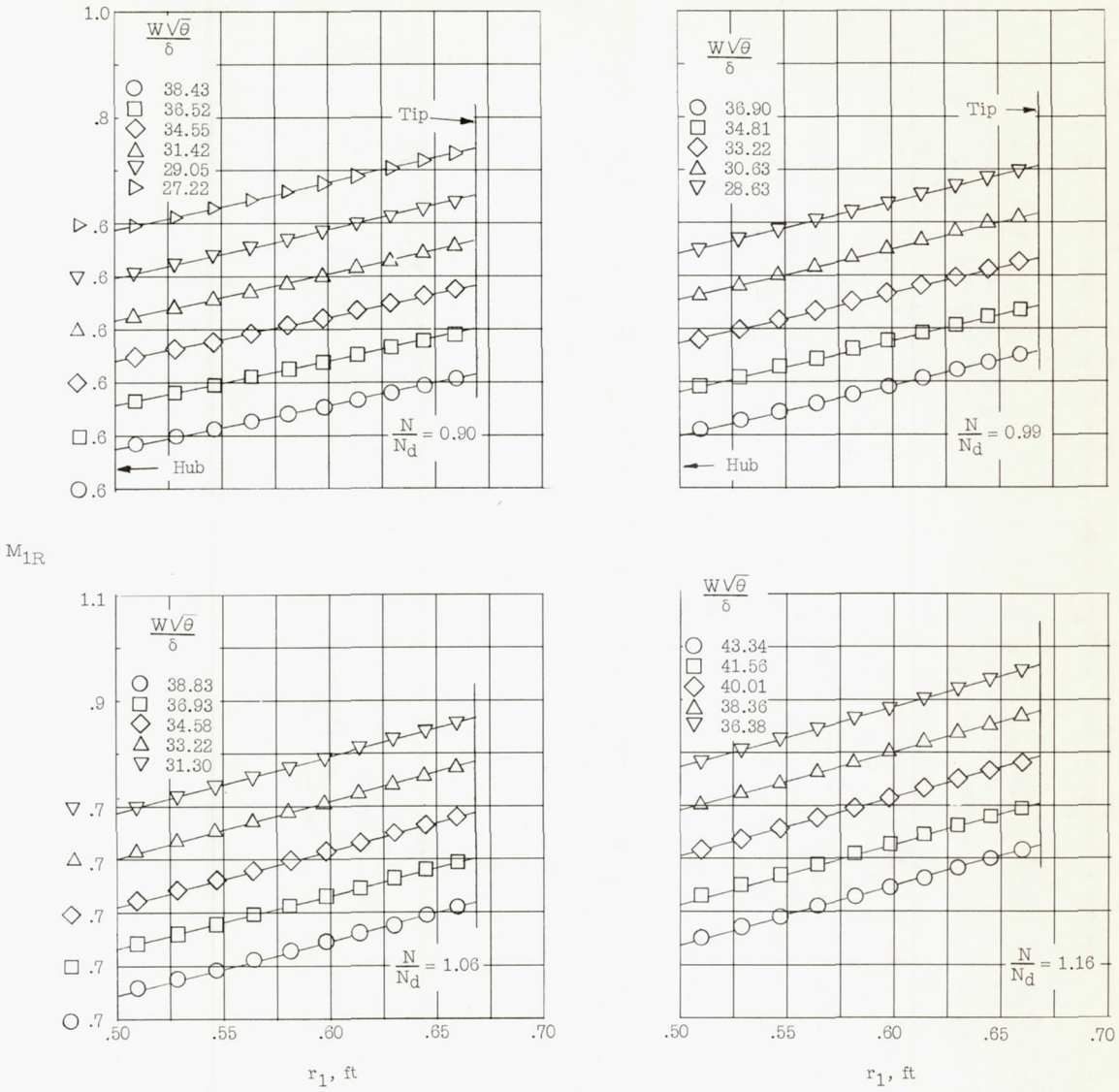

(a) $\frac{N}{N_d}$ = 0.90 to 1.16.

Figure 7.- Radial variation of inlet relative Mach number.

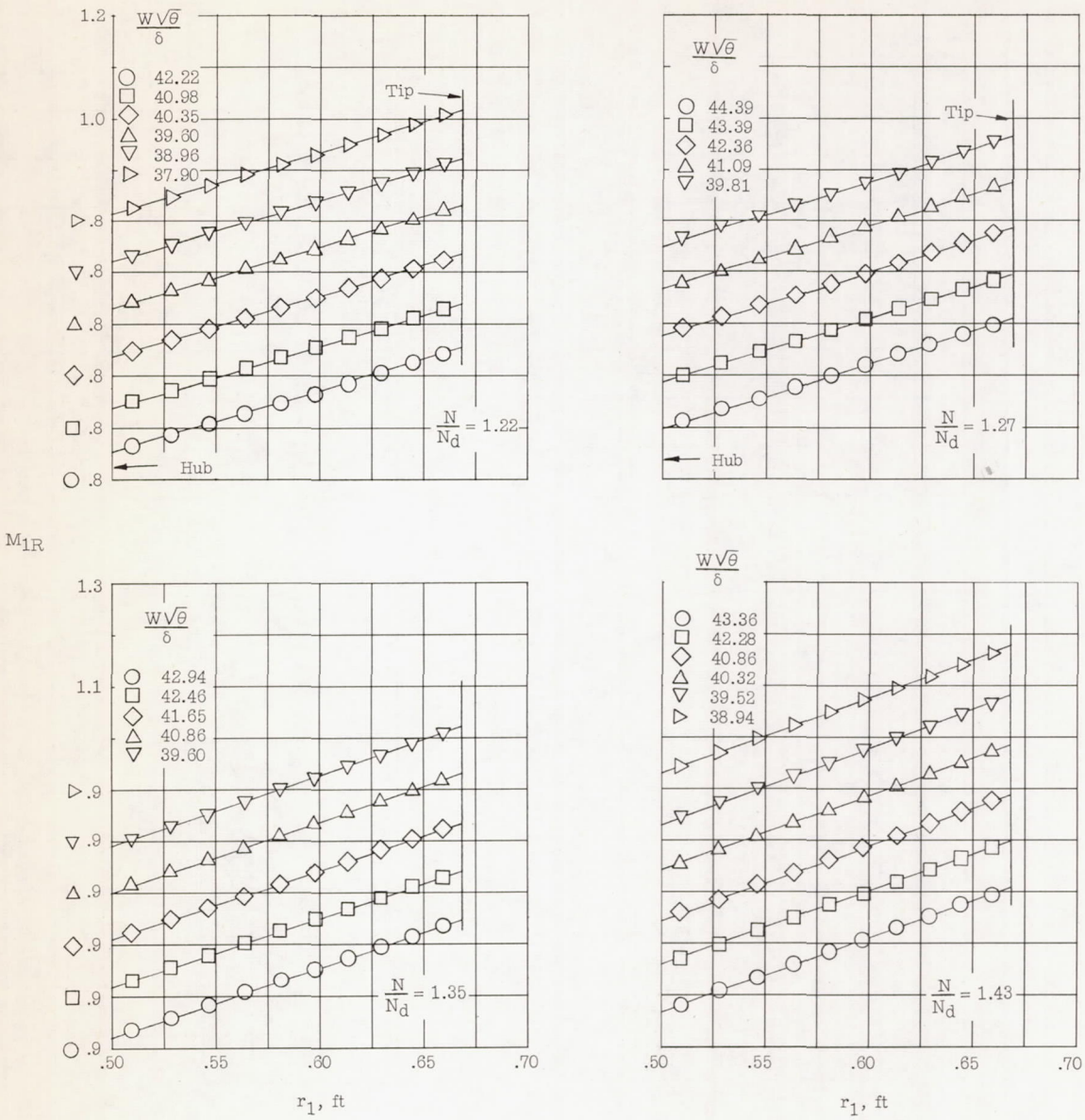

(b) $\frac{N}{N_d}$ = 1.22 to 1.43.

Figure 7.- Concluded.

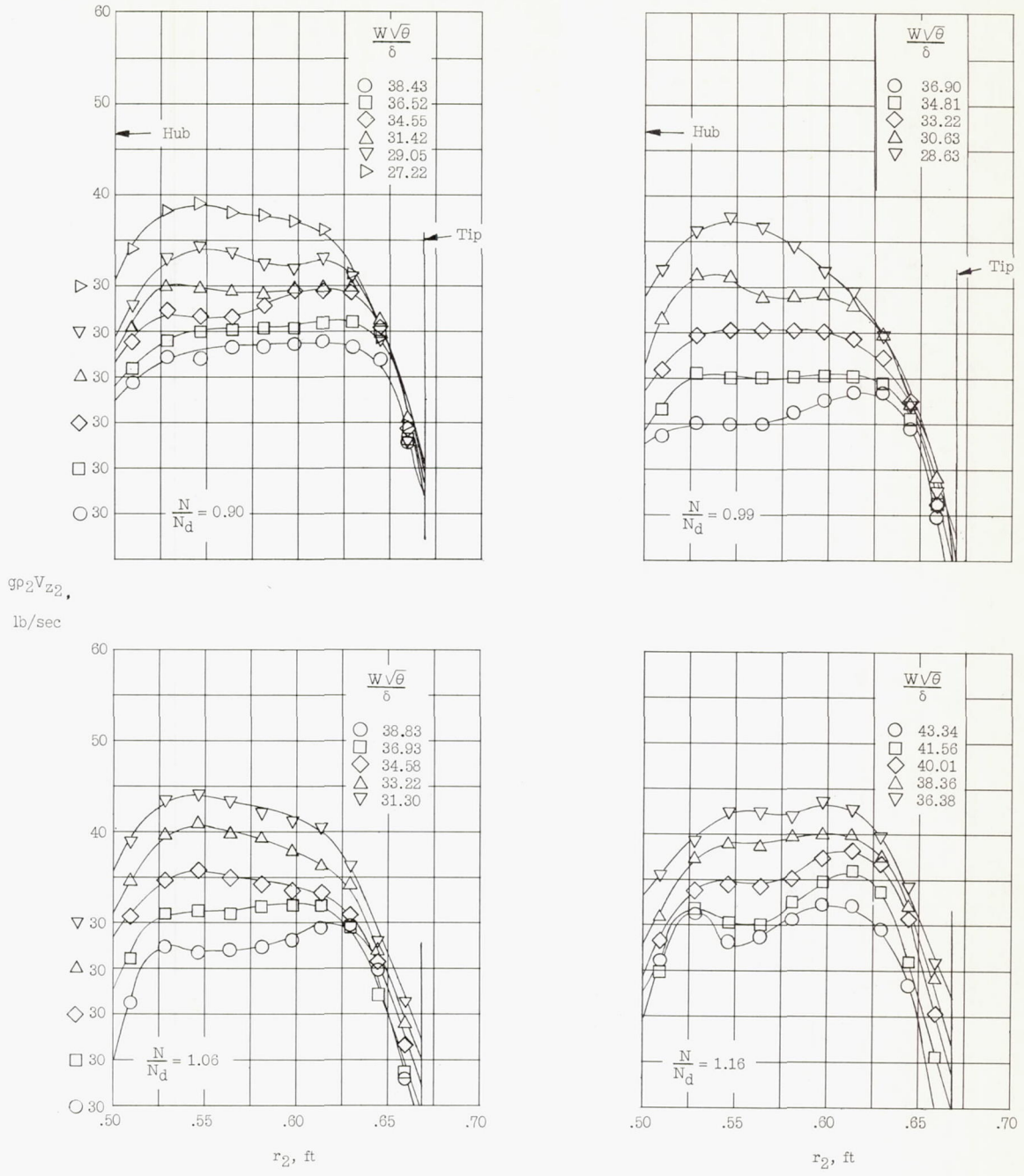

(a) $\frac{N}{N_d}$ = 0.90 to 1.16.

Figure 8.- Radial variation of mass flow leaving rotor.

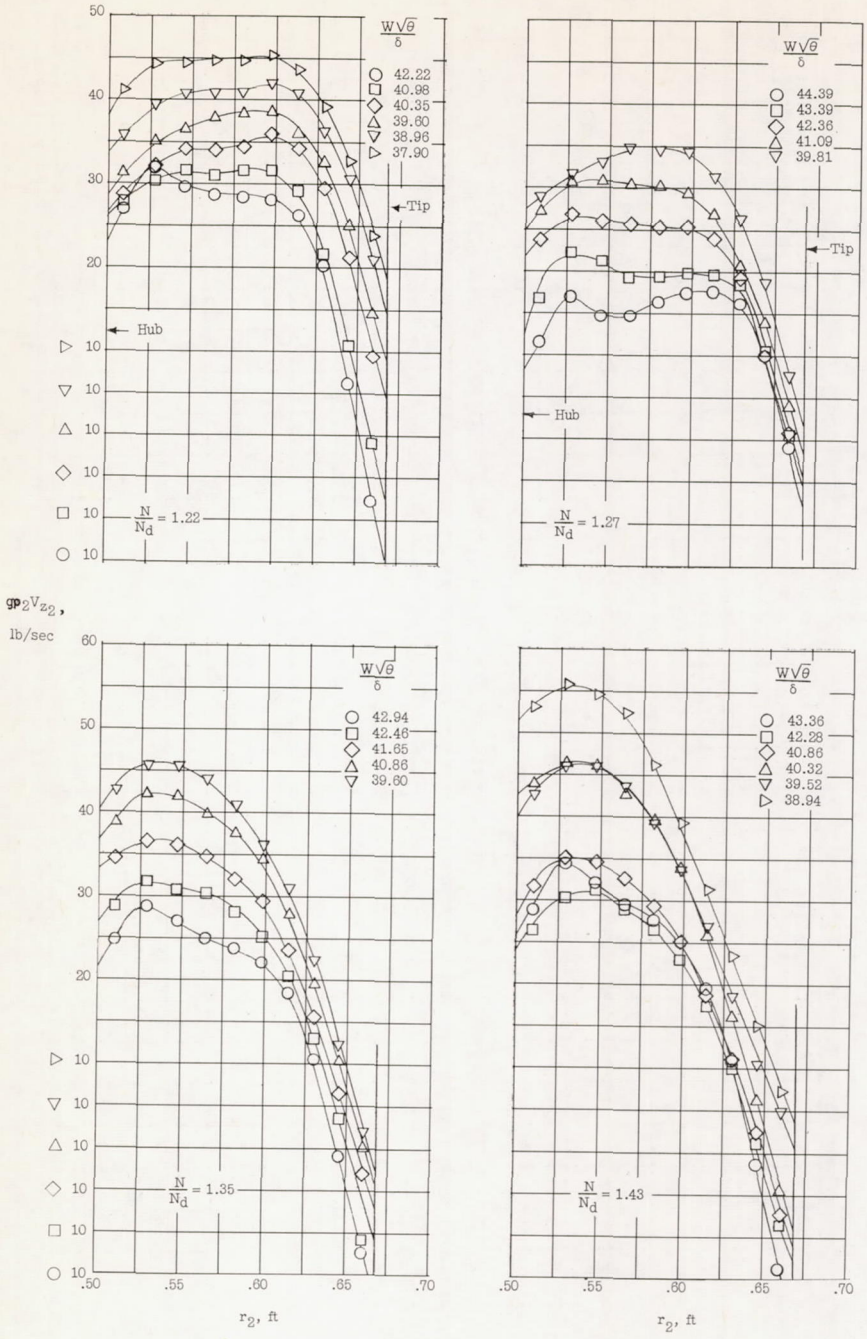

(b) $\frac{N}{N_d}$ = 1.22 to 1.43.

Figure 8.- Concluded.

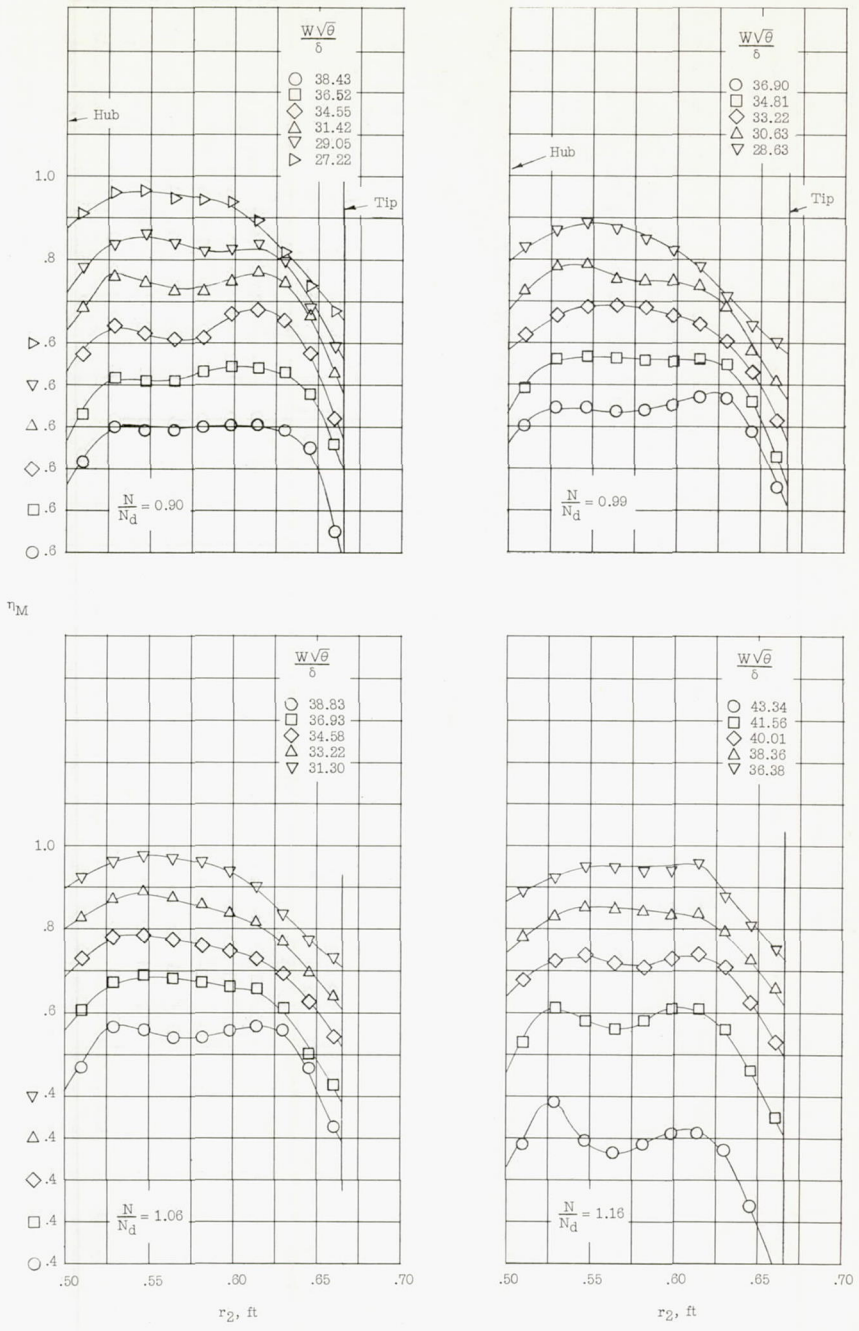

(a) $\frac{N}{N_d}$ = 0.90 to 1.16.

Figure 9.- Radial variation of momentum efficiency.

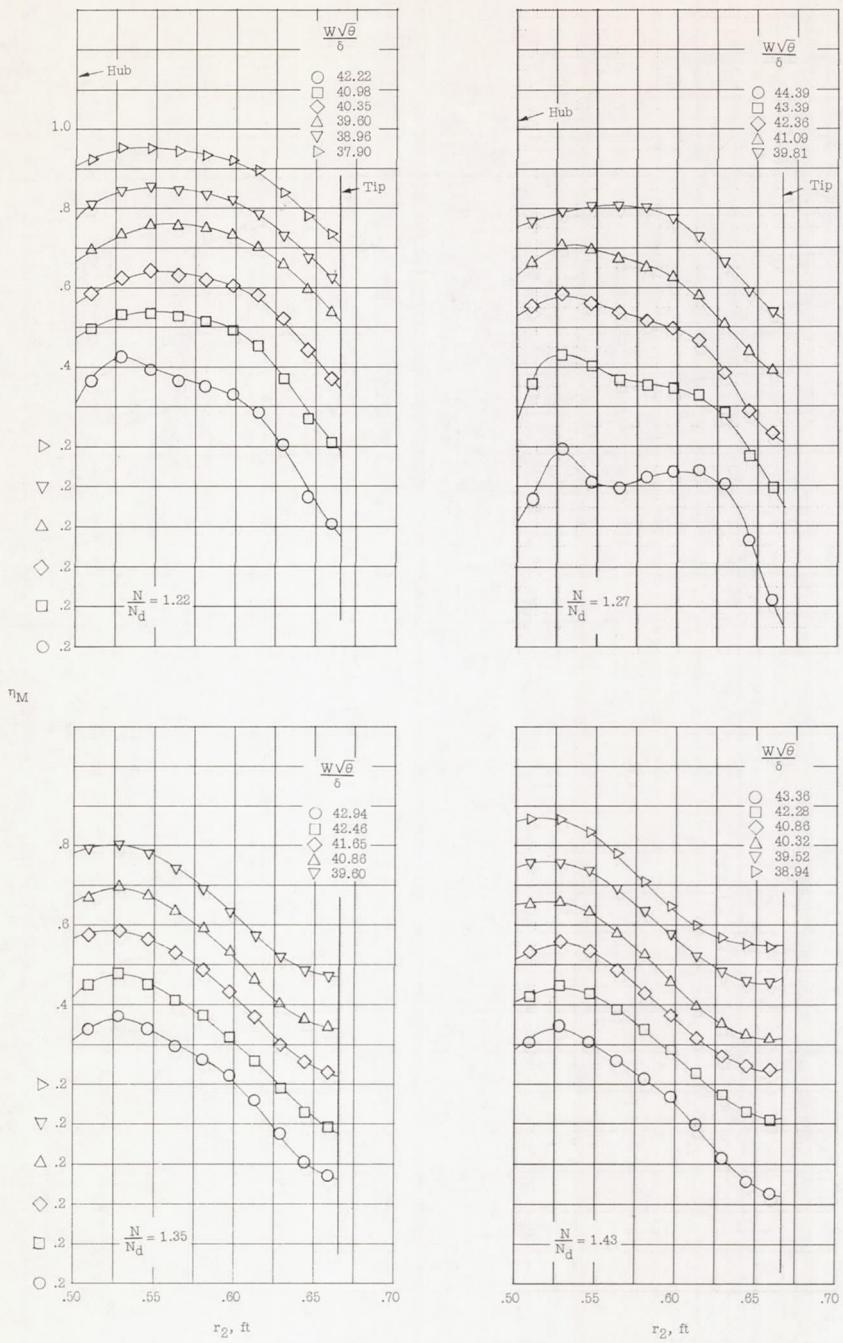

(b) $\frac{N}{N_d}$ = 1.22 to 1.43.

Figure 9.- Concluded.

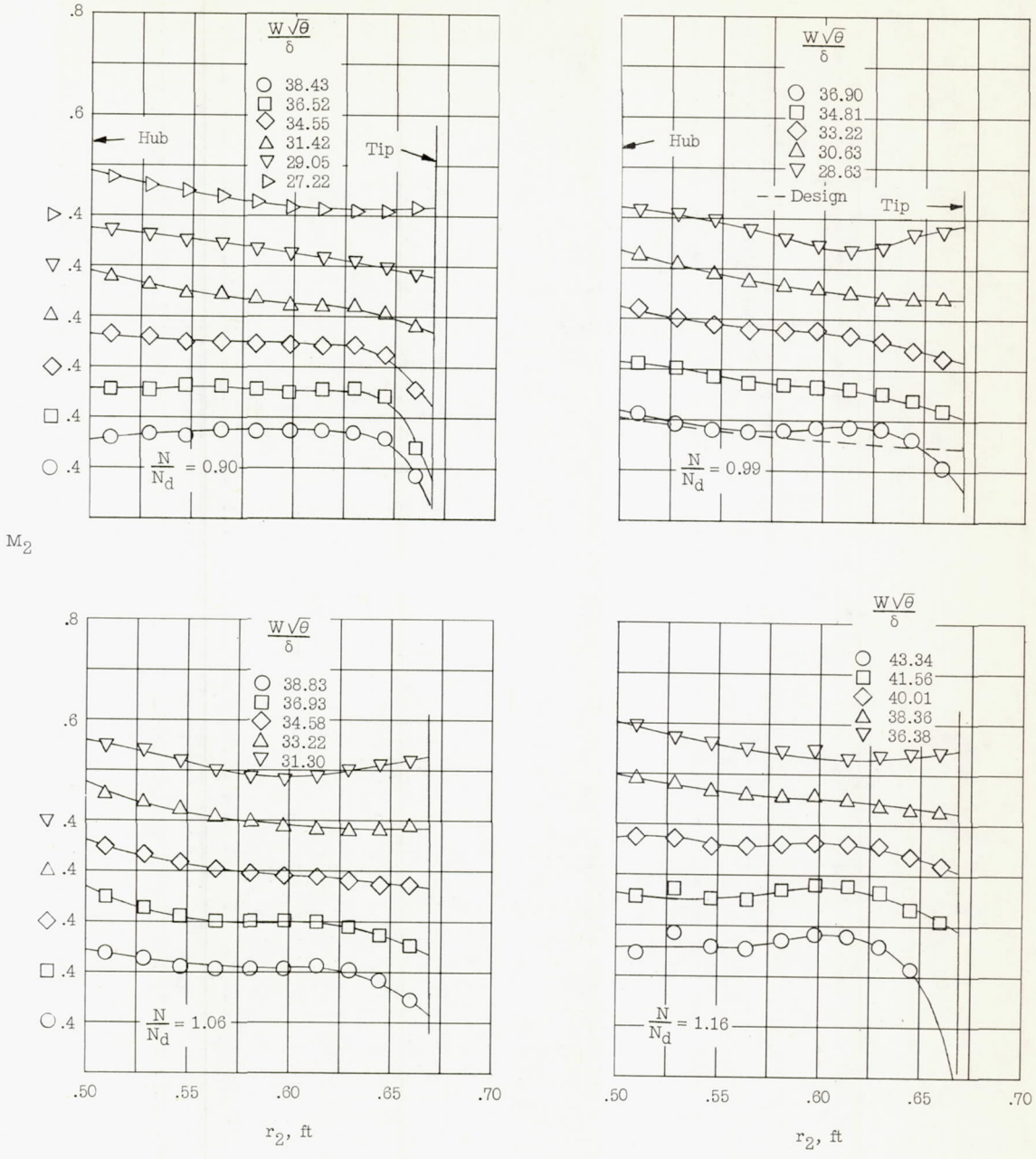

(a) $\frac{N}{N_d}$ = 0.90 to 1.16.

Figure 10.- Radial variation of absolute Mach number leaving rotor.

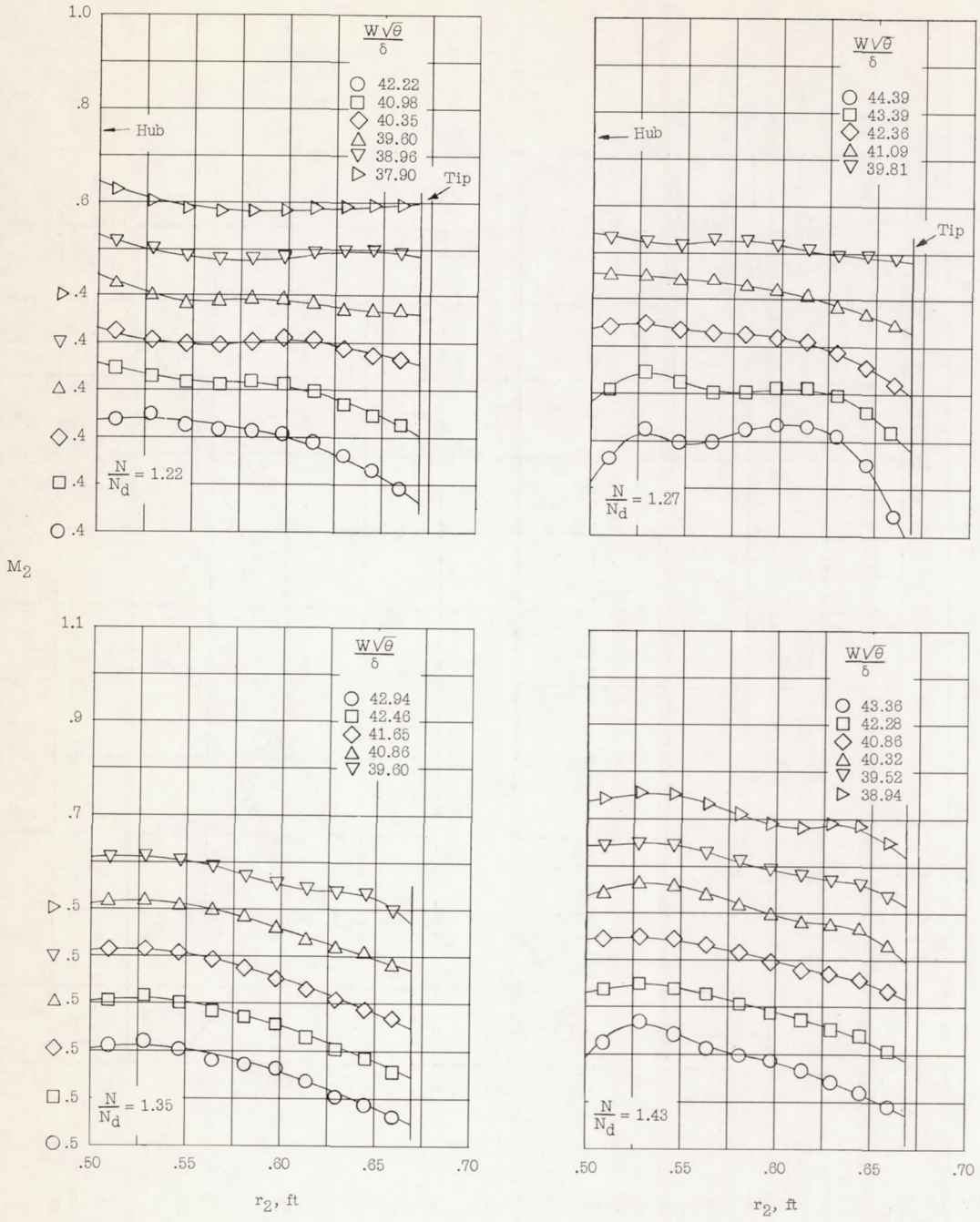

(b) $\frac{N}{N_d}$ = 1.22 to 1.43.

Figure 10.- Concluded.

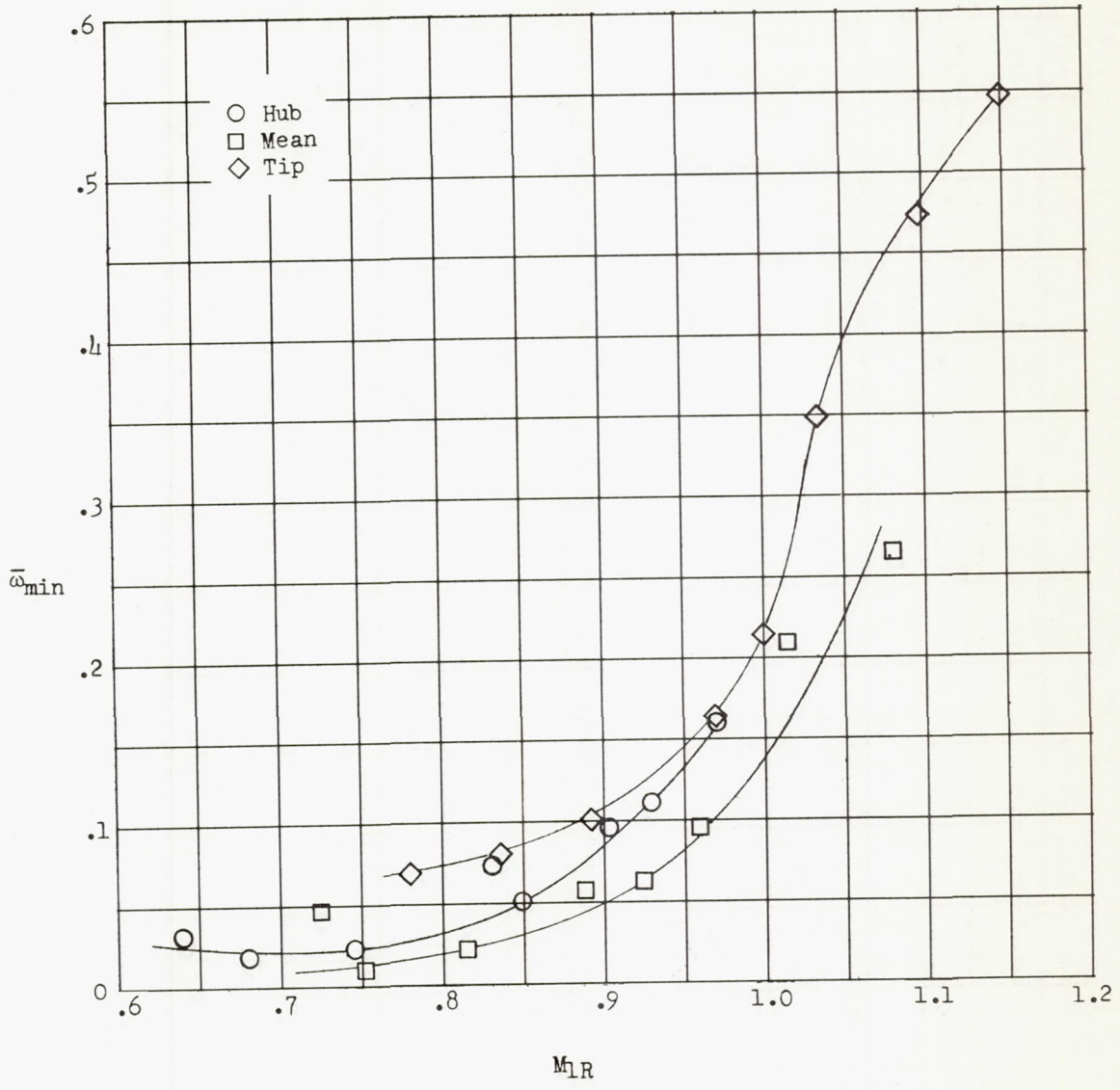

Figure 11.- Variation of minimum loss coefficient with inlet relative Mach number.

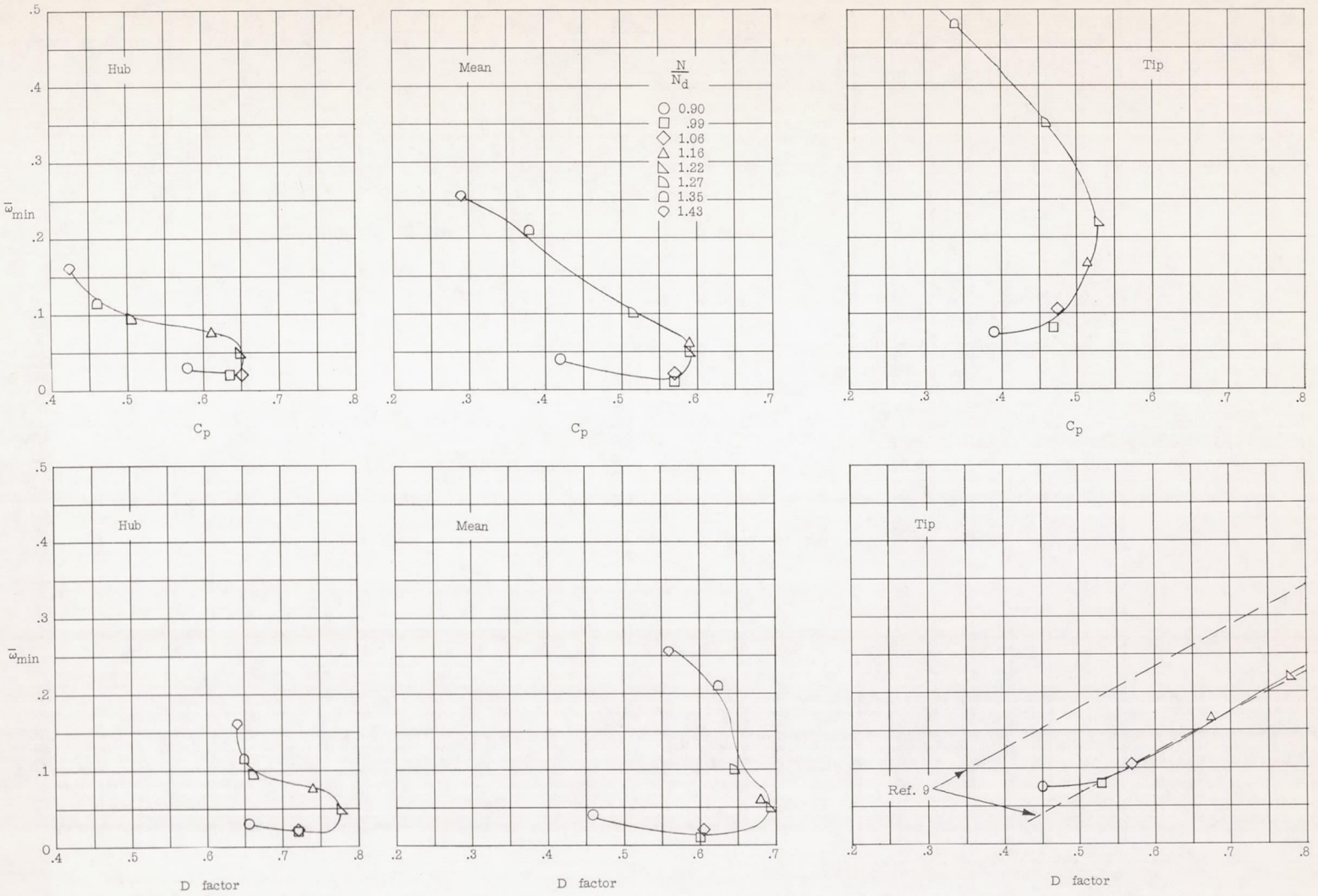

Figure 12.- Variation of minimum loss coefficient with D factor and static-pressure-rise coefficient at three blade elements.